UNIVERSIDADE FEDERAL DE ALFENAS

**Marcos Vinicius dos Santos**

# NEUTRINO INTERACTION AND DETECTION IN THE SBND EXPERIMENT

Poços de Caldas/MG
2018

**Marcos Vinicius dos Santos**

# NEUTRINO INTERACTION AND DETECTION IN THE SBND EXPERIMENT

Dissertação apresentada como parte dos requisitos para obtenção do título de Mestre em Física pelo Programa de Pós-Graduação em Física da Universidade Federal de Alfenas. Área de concentração: Física de partículas e campos. Orientador: Gustavo do Amaral Valdiviesso.

Poços de Caldas/MG
2018

Dados Internacionais de Catalogação-na-Publicação (CIP)
Sistema de Bibliotecas da Universidade Federal de Alfenas
Biblioteca campus Poços de Caldas

S237n Santos, Marcos Vinicius dos.
Neutrino interaction and detection in the SBND experiment / Marcos Vinicius dos Santos. -- Poços de Caldas/MG, 2018.
70 f. –

Orientador(a): Gustavo do Amaral Valdiviesso.
Dissertação (Mestrado em em Física) – Universidade Federal de Alfenas, campus Poços de Caldas, 2018.
Bibliografia.

1. Neutrinos. 2. Interações de neutrinos. 3. Partículas (Física nuclear). I. Valdiviesso, Gustavo do Amaral. II. Título.

CDD – 539.7215

Ficha Catalográfica elaborada por Thaís Aparecida de Lima
Bibliotecária-Documentalista CRB6/3032

Marcos Vinicius dos Santos

# Neutrino interaction and detection in the SBND experiment

A banca examinadora abaixo-assinada, aprova a Dissertação apresentada como parte dos requisitos para obtenção do título de Mestre em Física pelo Programa de Pós-Graduação em Física da Universidade Federal de Alfenas. Área de concentração: Física de partículas e campos.

Aprovada em: 11/10/2018

Prof.: Gustavo do Amaral Valdiviesso

Instituição: UNIFAL-MG

Assinatura:

Prof.: Fernando Gonalves Gardim

Instituição: UNIFAL-MG

Assinatura:

Prof.: Célio Adrega de Moura Junior

Instituição: UFABC

Assinatura: Célio A. Moura Jr.

Dedico esse trabalho aos meus pais, Rozili e Vicente e à minha vó Alexandrina, pelo apoio incondicional. Dedico também à minha querida Lais e meu irmão Julio.

# AGRADECIMENTOS

Eu admito que sou um mero coadjuvante desse trabalho, devido ao número de pessoas envolvidas direta e indiretamente em meu período de mestrado, mas farei o meu melhor para, em poucas linhas, lembrar de parte delas.

Primeiramente agradeço a natureza, por propiciar a oportunidade de investigá-la e preparar mistérios que instigam nós homens a olhar para o além horizonte. Quando digo natureza, também me refiro a Deus, o ser supremo que a planejou e preparou. Agradeço aos meus pais, Rozili e Vicente, à minha namorada Lais e meu irmão Julio, pelo apoio que transcende muito esses dois anos de preparação e por serem as melhores pessoas que conheci em minhas jornadas.

Jamais posso esquecer minha vó Alexandrina, que é a maior colaboradora para esse trabalho, sem ela, não espere que uma única linha dessa dissertação pudesse existir, e junto a ela minha tia Nenê, que foi uma pessoa muito especial nesses meus últimos anos, bem como seu marido Wilson.

Agradeço meu orientador e amigo Gustavo Valdiviesso, um dos melhores professores que já conheci, bem como uma das melhores pessoas. Sem dúvida segui com o mestrado por me inspirar nele. Agradeço por mostrar a beleza da física e por acreditar em mim quando nem eu mesmo acreditava, me proporcionando oportunidades nas quais me surpreendo até hoje por ter conseguido. Agradeço também à sua família, pelos ótimos momentos juntos no Fermilab.

De maneira nenhuma posso esquecer meu professor Fernando Gardim, pela paciência de acolher minhas dificuldades de forma muito bem humorada e precisa. Muito do que trabalhei aqui, se deve aos seus direcionamentos e correções. Se tiver a metade do seu conhecimento em física e em diplomacia um dia, serei um homem realizado.

Agradeço ao professor Leandro Lodi pelo seu voto de confiança e encorajamento, que mostrou a possibilidade de que esse trabalho poderia sair do mundo das minhas ideias. Sei que a maioria das pessoas deixa essa parte para o final, mas agradeço a UNIFAL-MG e a toda sua comunidade, por fazer essa instituição tão impactante na vida das pessoas. Sempre a terei como minha casa. Agradeço também aos docentes do PPGF, em especial aos professores Enrique, Cássius e Rodrigo e aos discentes Maria, Pablo, Farley, Fabiano, Danilo, George, Marcelo, Cado, Maurício, Carlos, Clayton, Gabriel e Silas que muito me ensinaram nesses últimos dois anos.

Agradeço também aos meus amigos especiais de Fermilab Felipe (Japa), Mônica, Miquéias, Vítor (Ronaldo), Renan (Locão), Andrea, Hector, Martin, Rijjesh, Etta, Raquel, Connor e Tom, a quem devo muito de minha dissertação, seja pela transmissão de conhecimento em física, seja pelo aprendizado do inglês, ou até mesmo pelo apoio emocional e ombro amigo em momentos fáceis e difíceis. Também agradeço meu amigo Ernesto e sua família, por bons momentos e churrascos juntos. Nessa mesma toada, agradeço ao

Fermilab, especificamente ao Neutrino Physics Center e especialmente a Ornella Palamara e Jen Raaf, por me proporcionarem a oportunidade única de colaborar pessoalmente com os experimentos SBND e LArIAT, onde vivi excelentes momentos por seis meses, tendo contato com ciência de ponta.

Não posso deixar de mecionar Gianluca Petrillo do Fermilab e Dominic Brailsford da Lancaster University, pela contribuição direta e extremamente relevante em minha análise.

Agradeço ao meu grande primo e amigo de todas as horas Gustavo, pelos infinitos (e prazerosos) momentos de discussão sobre física e política e as minhas fantásticas tias Socorro, Márcia, Do Carmo (e tio Zezinho), (também prima) Dani e sua família e à minha honorável vó Maria, que sempre estiveram ao meu lado, mesmo quando havia um oceano entre nós. Também agradeço aos meus amigos do peito Max e Cláudia, Mégda e Leandro, à quem tenho muito apreço.

Por fim agradeço à CAPES, ao Fermilab e ao Instituto de Ciência e Tecnologia da UNIFAL-MG, pelo apoio financeiro.

If I have seen further it is by standing on shoulders of giants.

(NEWTON, 1675)

Não me procure em uma lápide, eu estou aqui.

Autor

# ABSTRACT

The neutrino flavor oscillation phenomena is a conclusive proof of neutrino masses and can be described by a well established and tested quantum model. However, a non-completed part of this history lives in short-baseline experiments, due to LSND and MiniBooNE anomalies, with a possible fourth neutrino, heavier and devoid of flavor, therefore does not interact even weakly. SBN is a scientific program able to solve this short oscillation problem, using a high level of detection resolution, the LArTPC technology in three detectors, being the nearest from the source, SBND, the experiment with potential to make most precise measurement neutrino-argon cross section. Thus, this study is concentrated in understand neutrino interaction, in order to apply it in the SBND detection context. To achieve this goal, the $\nu_\mu - e^-$ scattering was used in a cross section calculation, where results showed the charged current process is not expected, given the energy threshold $\approx 11$ GeV, out of the SBN beam spectrum, while the neutral current scattering is allowed, but with a very low rate, due to the total cross section magnitude to be $\sigma_{NC} < 10^{-41} cm^2$, for energies $< 20$ GeV, that, compared to demonstrated neutrino-nucleus cross section at this energy range ($\approx 10^{-38}$ cm$^2$), is really small, so play a non-insignificant, but secondary hole in the experiment. After this overview, the simulation process with LArSoft was described and a sample of simulated data was used to show some physical expectations with truth information and at the end, detector simulation, which provides a more realistic response, allowing not only to test the current reconstruction algorithms, but also a particle identification tool. The development of the last one was part of the analysis, based in simple assumptions, such as track length and loss energy along space ($-dE/dx$) described by Bethe-Bloch equation, in a try of select muons, pions and protons in CC 0 and 1 $\pi^\pm$ in the final state channels. The results in general were positive, with $\approx 70\%$ efficiency in the case of all particles and individually in the muon and proton case, whose efficiency was $\approx 80\%$, but the pion efficiency was very low ($\approx 2\%$) and an hypothesis could be the presence of other particles do not considered or even the low number of assumptions to the algorithm making, that will need more detailed study for future works.



Keywords: Sterile neutrino. SBND experiment. Neutrino interaction. Neutrino detection.

# RESUMO

O fenômeno de oscilação de sabor de neutrinos é uma prova conclusiva da existência de sua massa e pode ser descrito por um bem estabelecido e testado modelo quântico. Contudo, uma parte incompleta dessa história vive em experimentos com curta baseline, devido uma anomalia medida nos experimentos LSND e MiniBooNE, com a possibilidade de um quarto neutrino, mais pesado e desprovido de sabor, portanto não interage nem fracamente. SBN é um programa científico capaz de resolver esse problema relacionado a curtas oscilações, usando um alto nível de resolução de detecção, a tecnologia LArTPC em três detectores, sendo o mais próximo da fonte, SBND, o experimento com potencial para fazer a mais precisa medição de seção de choque neutrino-argônio. Assim, este estudo está concentrado em entender a interação de neutrinos, de modo a aplicar esse conhecimento no contexto do experimento SBND. Para atingir esse objetivo, o espalhamento $\nu_\mu - e^-$ foi usado para um cálculo de seção de choque, onde os resultados mostraram que o processo que envolve corrente carregada não é esperado, dada a energia mínima para esse fenômeno ser $\approx 11$ GeV, fora do espectro de SBN, enquanto o espalhamento via corrente neutra é permitido, Mas com uma taxa de interações muito baixa, devido a seção de choque total ser da ordem de $\sigma_{NC} < 10^{-41}$ cm$^2$, para energias $< 20$ GeV, que, comparado com a seção de choque neutrino-núcleo nessa faixa de energia ($\approx 10^{-38}$ cm$^2$), é realmente pequena, então não desempenha um papel insignificante no experimento, mas que de qualquer forma é secundário. Após essa revisão do fenômeno de espalhamanto, o processo de simulção com LArSoft foi descrito e uma amostra de dados simulados foi utilizada para mostrar alguns resultados físicos com informação truth e por fim, a simulação do detector, que propicia respostas mais realísticas das interações de neutrinos, permitindo não apenas testar os algorítmos de reconstrução atuais, mas também uma ferramenta de identificação de partículas. O desenvolvimento desta última foi parte da análise, baseada em simples considerações, tal como o comprimento do track e energia perdida ao longo do espaço ($-dE/dx$) descrita pela equação de Bethe-Bloch, em uma tentativa de selecionar muons, pions e prótons no canal CC 0 e 1 $\pi^\pm$ no estado final. Os resultados em geral foram positivos, com eficiência de $\approx 70\%$ considerando todas as particulas e individualmente no caso do muon e do próton, no qual a eficiência foi de $\approx 80\%$, porém a eficiência para identificação de pions foi muito baixa ($\approx 2\%$) e uma hipótese para essa disparidade é a presença de outras partículas não consideradas ou até mesmo o baixo número de considerações para a construção do algorítmo de seleção, demandando um maior nível de detalhamento em trabalhos futuros.

Palavras-chave: Neutrino estéril. Experimento SBND. Interação de neutrinos. Detecção de neutrinos.

# LIST OF FIGURES

# LIST OF TABLES

# TABLE OF CONTENTS

# 1 INTRODUCTION

The Standard Model (SM) of particle physics is one of the most successful theories in science. Such agreement with a number of extensively tested experiments has opened a special world, allowing us to change our view of nature. The goals of this study belong in the context of the most evident, and still unsolved, issues in the SM. Namely those related to a very peculiar class of particles: neutrinos (BILENKY, 2015).

Neutrinos are elementary particles that do not interact via the Electromagnetic or Strong Forces, coupling only weakly with the vector bosons $W^{\pm}$ e $Z^0$ (as well as Gravity, but this source of interaction is many orders of magnitude weaker than the other fundamental forces)(FROGGATT; MUHEIM; SMITH, 2008). Since its proposal by W. Pauli in 1930, as a solution for a supposed violation of energy conservation in beta decays, neutrinos have been a challenging topic of research, experimentally and theoretically: they almost do not interact. As a reference, a neutrino with energy of about 1 TeV (high energy) can propagate in 2.5 million km of water without interacting, while lower energy ones could traverse light-years of lead, and still avoid interacting (GANDHI et al., 1998).

In the SM, neutrinos were originally considered *massless*, but later found to be *massive*, due to the well known flavor oscillation phenomenon, which is a periodic changing of neutrino flavor along space-time (WANG, 2018). The oscillation model was a way to solve the *neutrino solar problem*, a challenge that required many years in the second half of XX century and consisted in a difference between expected and measured neutrino flux from the sun and will be discussed in Section 2 (VALDIVIESSO, 2004).

Between the 1990s and 2000s, short baseline experiments as LSND and MiniBooNE observed an anomaly in the oscillation data, with an excess of measured $\nu_e(\bar{\nu}_e)$ from $\nu_\mu(\bar{\nu}_\mu)$ beams, indicating the possibility of an extra neutrino, which should be sterile, as we know from the invisible decay of the $Z^0$ boson that there is indications for 3 Weakly interacting neutrinos (DECAMP et al., 1989), with possibility for extensions of this assumption concerning interaction processes beyond the Standard Model (CARENA et al., 2003). In order solve this mystery, the Short Baseline Neutrino (SBN) program was proposed, composed by three different detectors, ICARUS (a.k.a. T600), MicroBooNE and SBND, (with baselines of 600 m, 470 m and 100 m respectively), all designed with the same technology, the Liquid Argon Time Projection Chamber (LArTPC) and located at Fermilab. The SBN program have capability to investigate the sterile hypothesis with high precision and it will be discussed in Section 3 (ANTONELLO et al., 2015).

The search for sterile neutrino is not the only scientific goal of SBN, since the LArTPC technology, important tool for the future of long baseline experiments such as DUNE (Deep Underground Neutrino Experiment), marks a revolution in precision particle physics. Being first developed by a team led by Nobel Prize laureate Carlo Rubbia, for the

ICARUS experiment in Italy, this technology enables high resolution tracking and particle identification, being scalable from a little larger than a shoe box (such as ArgoNeuT (ACCIARRI et al., 2017)) to the size of a cargo ship, such as DUNE. This technology will not only be extensively tested by the SBN program, accumulating experience for DUNE, but employed to obtain the most precise neutrino-argon cross-section measurement to date, via a combination of a high luminosity beam, optimal positioning, and large fiducial mass of the Short Baseline Near Detector (SBND), having the potential to answer important questions about neutrino interactions (ANTONELLO et al., 2015). The goal of this study is to become a road map for the understanding of neutrino cross sections in the SBND context.

The text itself was planned by the author to take the reader along a path as educational as possible, which might include novice readers, acting as a simple guide to future students in neutrino cross sections. The text is organized as follows: on Section 2 the mass-flavor mixing model is described as a solution to flavor oscillations; Section 3 gives the problematic where SBND experiment is involved, showcasing its detection technology; given the importance of understand neutrino interactions, the scattering channel $\nu_\mu + e^-$ was chosen as theoretical background for cross section calculation in 4.2 and 4.3, since this exhibit most of important characteristics for these phenomena; in 4.4, a simple summary of neutrino-nucleus scattering is shown, with no efforts to go deeply into nuclear models, which looks contradictory, given the importance of this phenomena for the thesis, but once the fundamental matters will be explained and considering the difficult range of energy that SBND is in ($\approx 0 - 3$ GeV), the study of nuclear models is out of the scope of this work; Section 5 will present the Monte Carlo simulation and analyze the results of a sample created by SBND collaboration, contemplating the use not only of powerful simulation tools, such as GENIE, but information of detector response for neutrino interactions in charged current interaction with and without a pion in the final state.

By the end, using all the learned abilities to connect neutrino interactions with neutrino detection, we present a discussion about particle recognition using the muon, pion and proton differences in a simple and yet relevant particle identification exercise, finally achieving the goals established here.

# 2 NEUTRINOS AND FLAVOR OSCILLATION

No way better to start any history than with a big mystery, mainly when the character is a ghostly figure that you never see, but appears when it is not expected. This is the perfect script describing neutrinos coming from the sun, where a big difference between measured and expected neutrino flux was an epic problem for particle physics during the final years of the last century. Turns out that solving it required a better understanding about what exactly is a neutrino. But first, let us go back to 1960s. There was a moment that highlighted a simple but very interesting fact: when a neutrino comes in and interacts inelastically with matter, it does necessarily creates either an electron or a muon among the secondary particles. It may be added to this picture that the tau also appears, at much higher energies. This led physicists to label neutrinos as $\nu_e$, $\nu_\mu$ and later $\nu_\tau$ depending on the channel of interaction. Of course this is just the beginning of this story, since these labels are recognized as leptonic flavors and are always conserved in interaction processes (GRIFFITHS, 2008). This fact was used as one of the assumptions to establish the Standard Solar Model (SSM), predicting the production of only electron neutrino flavor in the Sun, given that its energy density is not enough to create the muons or taus (VALDIVIESSO, 2004). Figure 1a shows the expectations from solar events over several targets, including Clorine (at Homestake), water (Kamiokande and Super Kamiokande), Gallium (SAGE, GALLEX and GNO) and heavy water (SNO). The observed rates in every experiment is consistently lower than the SSM prediction. What do they have in common? They can only observe charged current interactions, those that produce a lepton in the final state like mentioned before. Only after the first SNO neutral currents detections, those that are universal and can account for all flavors, was when the total number of predicted neutrinos was confirmed to be correct. Figure 1b shows the best fitted fluxes observed at the SNO detector, coming either from electron-neutrinos or from muon+tau-neutrinos (SNO et al., 2005). The conclusion was inescapable a fraction of the electron neutrinos produced in the Sun was changing flavors during its flight to the Earth, violating lepton flavor conservation.

One of the earliest hypothesis was proposed by Bruno Pontecorvo in 1957 that neutrinos could oscillate with its antiparticle (inspired in the oscillation of kaons, $K^0 \to \bar{K}^0$) was adapted to a possible changing of flavor. It could solve the solar deficit, but how? The quantum oscillation happens when two observables do not commute with each other and it will be anticipated to you: *mass* and *flavor*. It can be interpreted as a generalization of Heisenberg's uncertainty principle, so it is not possible to determine them simultaneously, hence, there is a quantum superposition of states as (VALDIVIESSO, 2008)

$$|\nu_l\rangle = U_{l_1} |\nu_{m_1}\rangle + U_{l_2} |\nu_{m_2}\rangle + U_{l_3} |\nu_{m_3}\rangle \,, \tag{1}$$

Figure 1 – Measurements of neutrino flux from the sun

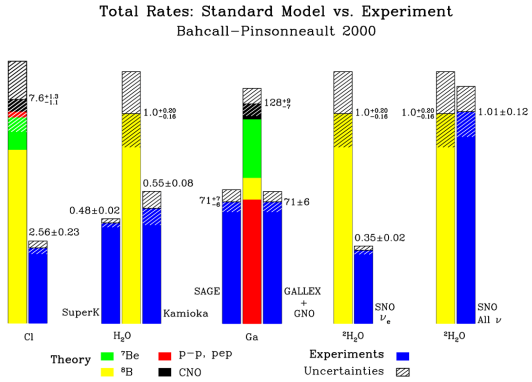


(a) Expected vs measured events in solar neutrinos experiments. The blue columns are the measured flux made by experiments and colored columns are number of expected neutrino events. Only SNO experiment was able to measures all neutrino flavors and was precise in the prevision of the flux, being most of them have a third of events.
Source: (FOGLI et al., 2006).

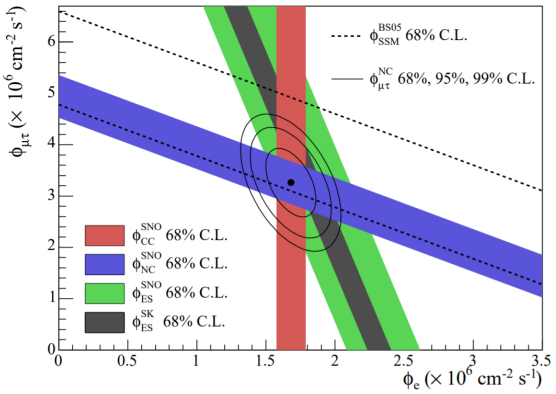


(b) Flux of $\nu_\mu$ and $\nu_\tau$ vs $\nu_e$. Dashed lines are the Standard Solar Model prediction. Solid bands are CC (charged current), NC (neutral current) and ES (elastic scattering) channels for SNO and Super Kamiokande experiments. The non-zero flux of $\nu_\mu$ and $\nu_\tau$ indicates an evidence of neutrino oscillations.
Source: (SNO et al., 2005).

in which, compactly, it is

$$|\nu_l\rangle = U_{lm}\,|\nu_m\rangle\,, \tag{2}$$

that can be rewritten in mass basis as

$$|\nu_m\rangle = U^{\dagger}_{ml}\,|\nu_l\rangle\,, \tag{3}$$

with $l = (e, \mu, \tau)$ being electron, muon and tau flavors and $m = (m_1, m_2, m_3)$, with $U_{lm}$ (or $U^{\dagger}_{ml}$) as an eigenvalue associated to the unitary operator applied on each eigenvector correspondent, ensuring the orthonormality between the two bases, therefore, a matrix with $U$ values respect

$$U^{\dagger}U = \mathbb{1}. \tag{4}$$

The matrix notation for all linear combinations will be

$$\begin{pmatrix} |\nu_e\rangle \\ |\nu_\mu\rangle \\ |\nu_\tau\rangle \end{pmatrix} = \begin{pmatrix} U_{e_1} & U_{e_2} & U_{e_3} \\ U_{\mu_1} & U_{\mu_2} & U_{\mu_3} \\ U_{\tau_1} & U_{\tau_2} & U_{\tau_3} \end{pmatrix} \begin{pmatrix} |\nu_{m_1}\rangle \\ |\nu_{m_2}\rangle \\ |\nu_{m_3}\rangle \end{pmatrix}, \tag{5}$$

and the unitary operator in equation (5) allows the interpretation of $U$ matrix to be a rotation and is known mixing matrix.

To represent a neutrino time evolution, it is possible to use Schrödinger equation in mass basis (to get a well defined neutrino energy), thus

$$i\frac{\partial}{\partial t}\left|\nu_m(t)\right\rangle = \widehat{H}\left|\nu_m(t)\right\rangle, \tag{6}$$

where (6) is in natural units[1]. But, is the mass base the responsible to interact from massive bosons to Weak Interaction? The answer is no: this is a feature of the flavor eigenstates and neutrino detectors are more interested on this observable.

It is possible to handle with only two flavors and two masses, making $f = (\mu, \tau)$, in order to simplify our analysis. So, (5) becomes

$$\begin{pmatrix} |\nu_e\rangle \\ |\nu_f\rangle \end{pmatrix} = \begin{pmatrix} \cos\theta & \sin\theta \\ -\sin\theta & \cos\theta \end{pmatrix} \begin{pmatrix} |\nu_{m_1}\rangle \\ |\nu_{m_2}\rangle \end{pmatrix}. \tag{7}$$

Solving the Schrödinger equation using mass eigenvectors for $|\nu_{m_1}(t)\rangle$ and $|\nu_{m_2}(t)\rangle$, are obtained

$$|\nu_{m_1}(t)\rangle = \nu_{m_1}(0)e^{-iE_1 t} \tag{8}$$

and

$$|\nu_{m_2}(t)\rangle = \nu_{m_2}(0)e^{-iE_2 t}. \tag{9}$$

It is possible to imagine the situation where are generated only electron neutrinos (as in the sun), thus $\nu_e(0) = 1$ and $\nu_f(0) = 0$, resulting in $|\nu_{m_1}(0)\rangle = \cos\theta$ and $|\nu_{m_2}(0)\rangle = \sin\theta$ from (3) and (7). For electron neutrino flavor, the equation (1) for 2 masses becomes

$$|\nu_e(t)\rangle = \cos\theta\,|\nu_{m_1}(t)\rangle + \sin\theta\,|\nu_{m_2}(t)\rangle \tag{10}$$

that can be multiplied by the corresponding bra from the left, as well as used (8) and (9), the result is

$$\begin{aligned} |\,\langle\nu_e(t)|\nu_e(t)\rangle\,|^2 \quad &= |\cos^2\theta\,\langle\nu_{m_1}(t)|\nu_{m_1}(t)\rangle + \sin^2\theta\,\langle\nu_{m_2}(t)|\nu_{m_2}(t)\rangle + \\ &\sin\theta\cos\theta(\langle\nu_{m_1}(t)|\nu_{m_2}(t)\rangle + \langle\nu_{m_2}(t)|\nu_{m_1}(t)\rangle\,|^2 \\ &= |\cos^4\theta + \sin^4\theta + \sin^2\theta\cos^2\theta[e^{-i\Delta E_{21}t} + e^{i\Delta E_{21}t}]|^2, \end{aligned} \tag{11}$$

[1] it is important the mention that throughout text will be developed using natural units, except when specified another System opf Units.

where $\Delta E_{21} = E_2 - E_1$. Using Euler's identity it is possible open exponential terms to

$$= \quad |\cos^4\theta + \sin^4\theta + \sin^2\theta\cos^2\theta[-i\sin(\Delta E_{21}t) +$$

$$\cos(\Delta E_{21}t) + i\sin(\Delta E_{21}t) + \cos(\Delta E_{21}t)]|^2 \tag{12}$$

$$= |\cos^4\theta + \sin^4\theta + 2\sin^2\theta\cos^2\theta\cos(\Delta E_{21}t)|^2,$$

and finally, it is possible to use the trigonometric relations

$$2\sin a\cos a = \sin(2a) \tag{13}$$

$$\cos a = 1 - 2\sin^2(2a) \tag{14}$$

where the result, so called Survivor Probability, is a statistical entity able to quantify the flavor oscillation along of time (VALDIVIESSO, 2008)

$$P_{\nu_e\to\nu_e}(t) = 1 - \sin^2 2\theta\sin^2(\Delta E_{21}t)\,. \tag{15}$$

The total energy can be related with momentum and mass as

$$|\boldsymbol{p}| = E\left(1 - \frac{m^2}{E^2}\right)^{1/2} \approx E - \frac{m^2}{2E}, \tag{16}$$

which was applied Taylor Series for $m^2/E \ll 1$. This result shows that

$$\Delta E_{21} = |\boldsymbol{p}_2| + \frac{m_2^2}{2E} - |\boldsymbol{p}_1| - \frac{m_1^2}{2E} = \frac{\Delta m_{21}^2}{2E}, \tag{17}$$

that is an implicit result, with $E$ interpreted as a neutrino beam energy and $|\boldsymbol{p}_1| = |\boldsymbol{p}_2|$ in the relativistic limit, with $x = t$ in natural units, (15) change to an evolution in space as

$$P_{\nu_e\to\nu_e}(x) = 1 - \sin^2 2\theta\sin^2\left(\frac{\Delta m_{21}^2}{2E}x\right). \tag{18}$$

Table 1 – Neutrino Oscillation parameters[a]

| Mixing angles | $\Delta m^2$ |
|---|---|
| $\sin^2\theta_{12} = 0.304 \pm 0.014$ | $\Delta m_{21}^2 = (7.53 \pm 0.18) \times 10^{-5} eV^2$ |
| $\sin^2\theta_{23} = 0.51 \pm 0.05$ | $\Delta m_{32}^2 = (2.44 \pm 0.06) \times 10^{-3} eV^2$ |
| $\sin^2\theta_{13} = (2.19 \pm 0.12) \times 10^{-2}$ | $\Delta m_{31}^2 = \Delta m_{32}^2 + \Delta m_{21}^2$ |

[a] Considered parameters with only normal mass hierarchy.

Source: author, using parameters from (PATRIGNANI; GROUP et al., 2016).

Figure 2 – Survivor probability for initials electron, muon and tau neutrinos

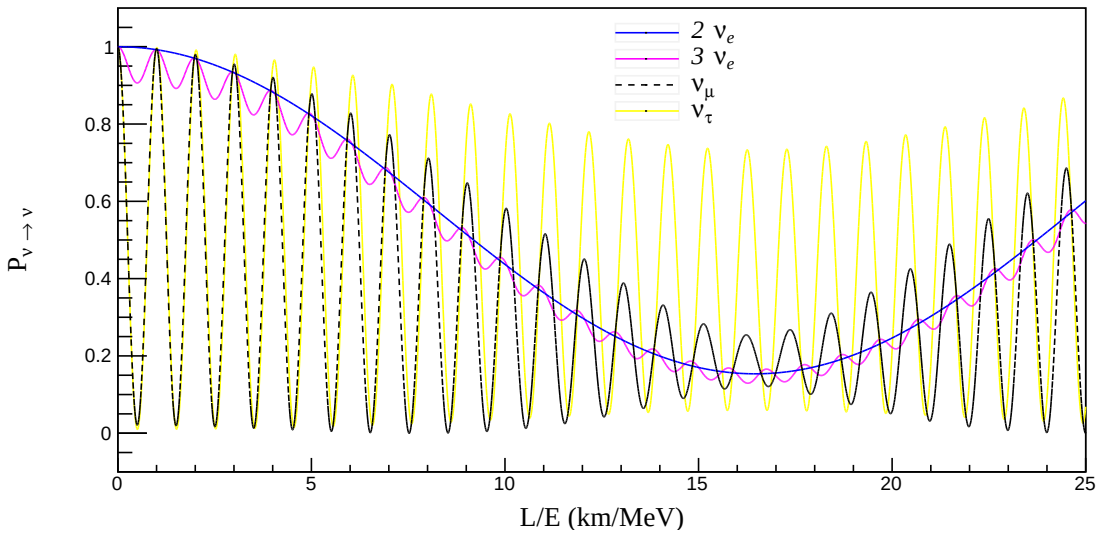


Blue line represents the 2 families approximation from equation (18) (in SI units), whereas other lines consider the complete model using the mixing matrix from (5) and parameters from Table 1.
Source: author.

Figure 3 – Survivor probability for initial electron neutrino

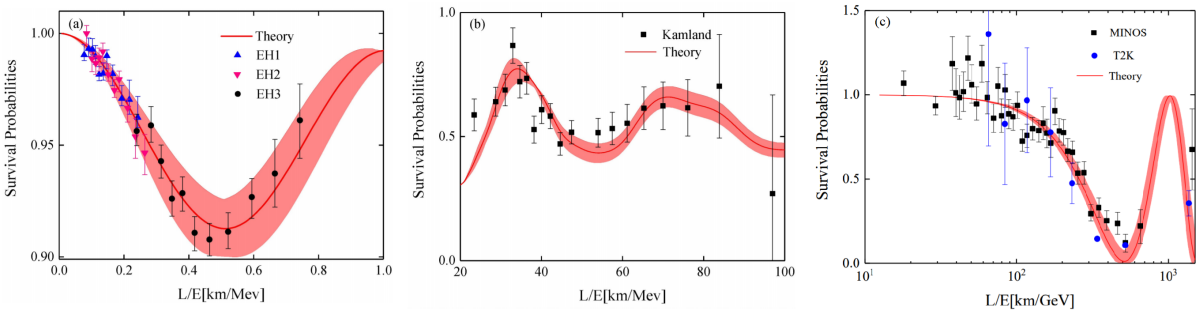


(a) Daya Bay experiment, (b) Kamland experiment and (c) MINOS and T2K, starting from short to long range, considering the ratio $L/E$, respectively. The red band represents a confidence level of $3\sigma$.
Source: (SONG et al., 2018).

Equation (18), described by Figure 2, has an astonishing implication: whether neutrinos are massless particles, the second term of (18) is null and the flavor is conserved in their propagation, with $P_{\nu_e \to \nu_e} = 1$. Experiments along of the decades have shown that the oscillation really occurs, so they do have mass[2]. Figure 3 shows four experiments with data agreeing with the oscillation model described in different scales of propagation ($L$ in km) in a spectrum of energy.

[2] It haven't been experiments able to measure neutrino mass(es), such low magnitude. The accessible values are only the $\Delta m^2$.

Considering a model with three neutrinos, two more $\theta_{ij}$ and $\Delta m^2_{ij}$ appears, already very well measured as shown in Table 1, solidifying the existence of the oscillation phenomenon. However, short baseline experiments, such as LSND and MiniBooNE, have measured an anomalous shorter period of oscillation, with the parameters space allowing a greater $\Delta m^2 \approx 1eV^2$. Next section will discuss this problem.

# 3 SHORT BASELINE NEAR DETECTOR (SBND) EXPERIMENT

Figure 4 – LSND $\bar{\nu}_e$ events (neutrino interactions detected) excess that indicates an unexpected $\bar{\nu}_\mu \rightarrow \bar{\nu}_e$ appearance

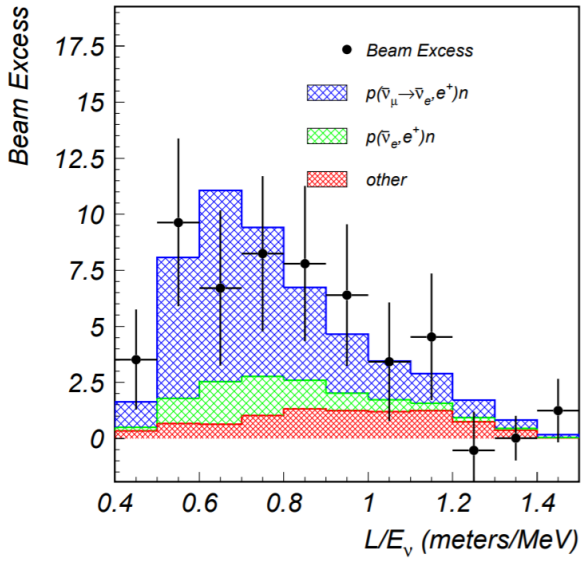


Bars refers to statistical and systematical error. Note that comparing the graph scale to Figure 2 there is a change of three orders of magnitude (km $\rightarrow$ m) to the size of the baseline, bringing the shorter oscillation idea.
Source: (AGUILAR et al., 2001; CONRAD; SHAEVITZ, 2016).

The picture established for the oscillation model has given consistency to three flavor neutrinos ($\nu_e$, $\nu_\mu$, $\nu_\tau$) and three different masses eigenstates ($\nu_1$, $\nu_2$, $\nu_3$). But in the 1990s with LSND (Liquid Scintillator Neutrino Detector) and the next decade with MiniBooNE, two accelerator based and specifically short-baseline experiments, detected an electron-like excess out of Standard Model prediction (Figures 4 and 5) (AGUILAR et al., 2001; AGUILAR et al., 2009). The key to understand this anomaly starts in the neutrino beam, that in general is generated by a proton beam striking a target, creating charged pions, with decay mode being $\simeq 99.98\%$ to $\mu^\pm + \nu_\mu(\bar{\nu}_\mu)$ (PATRIGNANI; GROUP et al., 2016). The consequence is that the initial neutrino beam is composed mostly by $\nu_\mu$ and Figure 2 shows that almost no oscillation is expected at short range distances such LSND and MiniBooNE[3], which implies, for conservation of lepton number, a considerably higher number of muon-like events than the electron ones (MINIBOONE et al., 2008). The hypothesis is a possible new eigenstate $\nu_4$, giving a new $\Delta m^2 \sim 1\ eV^2$, higher than the ones in Table 1, which implies a lower oscillation length and the existence of a new neutrino, devoid of leptonic flavor, thus, named sterile, would be unable to interact even weakly (CONRAD; SHAEVITZ, 2016; COLLIN et al., 2016).

[3] LSND and MiniBooNE are $\simeq 30\ m$ and $\simeq 540\ m$ from the neutrino source respectively (MINIBOONE

Figure 5 – MiniBooNE distribution (a) and excess (b) of $\nu_e$ events

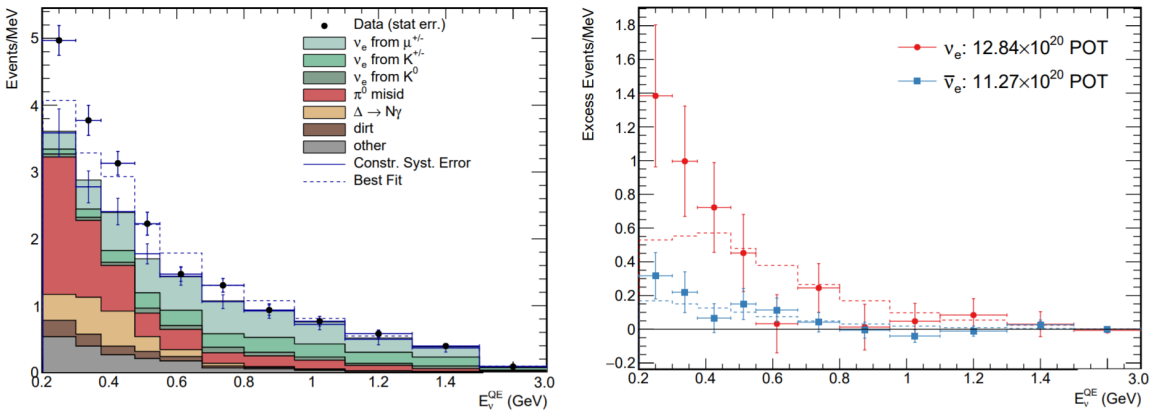


(a) $\nu_e$ events distribution

(b) $\nu_e$ and $\bar{\nu}_e$ events excess

$12.84 \times 10^{20}$ POT in a spectrum of energy, considering Quasi-Elastic scattering channels. Blues points on (b) represents antineutrino-mode data.
Source: (AGUILAR et al., 2018).

Around that mystery, was born a proposal for investigating the existence of sterile neutrino, Short Baseline Neutrino (SBN) Program is a huge scientific initiative situated on Fermi National Accelerator Laboratory (Fermilab) in Illinois, USA, consisting in three detectors (a fact able to reduce considerably systematic uncertainties (ANTONELLO et al., 2015)) crossed for the well studied Booster Neutrino Beam (BNB) along $\sim$ 1 km: ICARUS-T600, MicroBooNE and SBND, localized 600 m, 470 m and 110 m respectively from the source, will give precisely the oscillation behavior for short distances. The three experiments are based in LArTPC technology.

Besides the sterile neutrino investigation, SBND will collect the highest number of interactions already measured in an experiment, giving possibly the most precise neutrino-argon cross section measurement, with a total of $\sim 6.6 \times 10^{20}$ POT of exposure[4] in the 112 ton of active mass detector, with a volume of 4 m (width) $\times$ 4 m (height) $\times$ 5 m (length, beam direction) (ANTONELLO et al., 2015). The dominant channel (or topology[5]) is the CC $0\pi$ (Charged Current with no pion produced in the interaction), where more than 3 million of events are expected. These facts put the neutrino interactions as a crucial understanding to achieve SBN goals, mainly with regard neutrino-nucleus scattering, that intrinsically depends on the neutrino energy and has a complex theoretical picture, due to its composite nature described for a set of models, but the same target of the three

et al., 2008).

[4] The expression POT refers to Protons On Target, which means how many protons the accelerator has to scatter off a specific target (for BNB is composed by beryllium) to generate the amount of neutrino flux.

[5] The terms channel, or topology mean the combination of particles in the final state to be detected, generating a particular combination of tracks those are expected to be generated by a specific physical process.

Figure 6 – Allowed regions (right hand side of the lines and colored area) for $\Delta m^2_{41} \times \sin^2 2\theta$ of MiniBooNE experiment

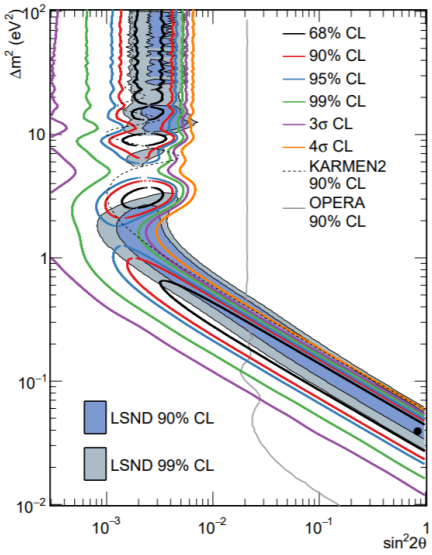


MiniBooNE correspond non specified lines, whereas LSND, OPERA and KARMEN2 are specified.
Source: (AGUILAR et al., 2018).

Figure 7 – (a) Flux expected on SBND experiment and (b) ratio between fluxes expected in ICARUS and SBND taken from the experimental project

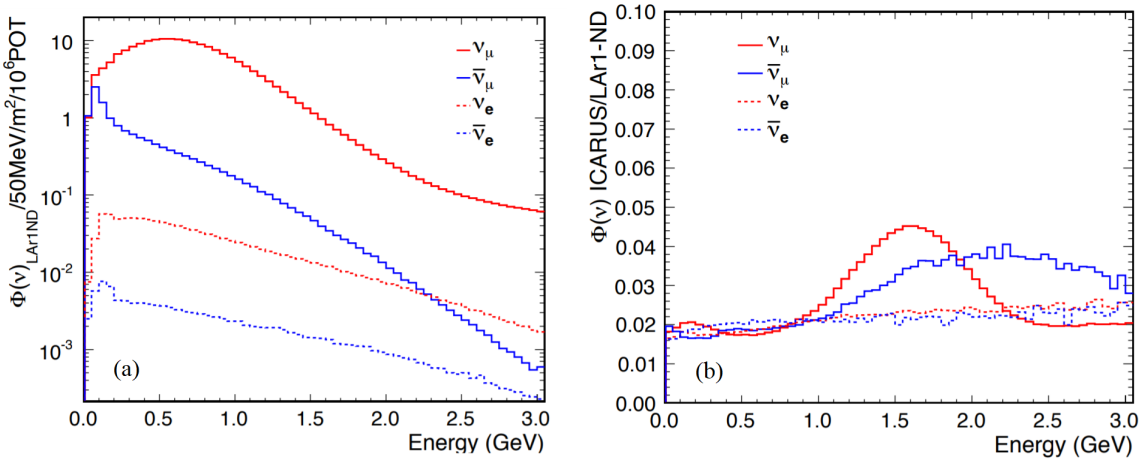


For each $\nu_\mu$ a $\mu^+$ is created in the beam, which decays into $e^+ + \nu_e + \bar{\nu}_\mu$ (PATRIGNANI; GROUP et al., 2016) explaining the majority of the contamination. Important the mention of the $\bar{\nu}_\mu$ contamination (and also $\nu_e$ and $\bar{\nu}_e$ in lower quantities) generated by the beam design. The same Figure shows a peak of flux around 700 MeV. Note that the first name proposed for SBND was LAr1-ND.
Source: (ANTONELLO et al., 2015).

detectors can reduce the uncertainties coming from the nuclear interactions. Section 4 is going to discuss this important sector in the evolution of the neutrino oscillation programs.

The detection strategy is measure the possible $\nu_e$ appearance ($\nu_\mu \rightarrow \nu_e$) and $\nu_\mu$

disappearance ($\nu_\mu \to \nu_\mu$) along the short baseline, testing the 3+1 models, with survivor probability

$$P^{3+1}_{\nu_\mu \to \nu_e} = 1 - \sin^2 2\theta_{\mu e} \sin^2 \left( \frac{\Delta m^2_{41}}{2E} L \right) \tag{19}$$

and

$$P^{3+1}_{\nu_\mu \to \nu_\mu} = 1 - \sin^2 2\theta_{\mu\mu} \sin^2 \left( \frac{\Delta m^2_{41}}{2E} L \right) \tag{20}$$

that can be used to measure $\Delta m^2_{41}$ range. Figure 6 shows allowed regions for this parameter in a number of oscillation experiments, correlating it with the mix angle. The scientific goals of SBN (in which are detailed in (ANTONELLO et al., 2015)) are also connected to the important task to prepare the science and technology of LArTPCs to long baseline experiments as DUNE.

The LArTPC is a very efficient detection system, with high performance of resolution and particle recognizing, uses the argon as a target for the neutrino, given the chemical instability and availability (argon is by far the cheapest noble gas), being ideal to use in neutrino experiments. Figure 8a shows the scheme, which can be summarized in the following steps (ANTONELLO et al., 2015):

1. The neutrino interacts to liquid argon, charged particles are created;
2. The charged particles transverse the medium and leave an ionization trace;
3. An electric field drifts the electrons to the wall, which pass through wire chambers leaving a induction signal (by induction plane(s)), until being collected (by the collection plane);
4. The drift time of the charges is given from the moment when the ionization starts, since photons are generated, which are collected by a photon detection system, composed mainly by PMTs into the detector;

The resulting entity from this process is the perturbation on the wires, or hits, those are equivalent to a peak of charge as shown in Figure 8b. The combination of the signals provides a 3D track[6] with a color level scale meaning the density of charges. The integration of the hits gives the energy loss with high performance of calorimetric resolution and then, particle identification.

Figure 9 shows a neutrino detection from MicroBooNE experiment, giving an idea of the high resolution of LArTPCs.

[6] The track is a trace (or combination of traces) of charges generated by the interaction of secondary charged particles in the medium.

Figure 8 – LArTPC detection scheme

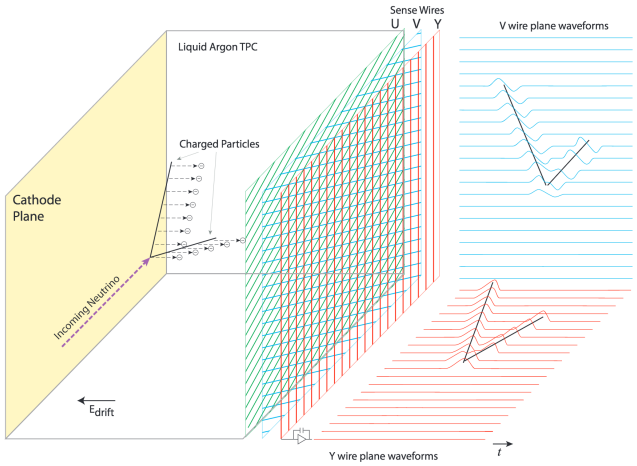


(a) Liquid Argon Time Projection Chamber (LArTPC) in the context of neutrino detection.

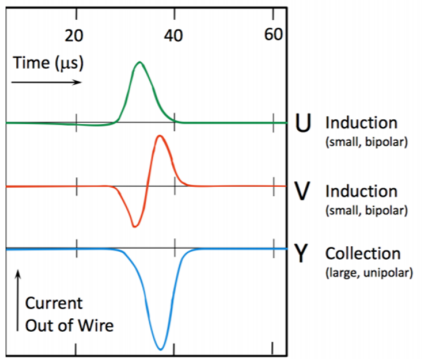


(b) Signals from charges on induction and collection planes. X axis represents their drift time.

Both figures show the detector perturbation due to neutrino interaction, where charges are drifted and are measured by induction and collection planes of wires.
Source: (ABRATENKO et al., 2017) and (PARTYKA, 2013).

Figure 9 – Neutrino interaction detected by MicroBooNE experiment

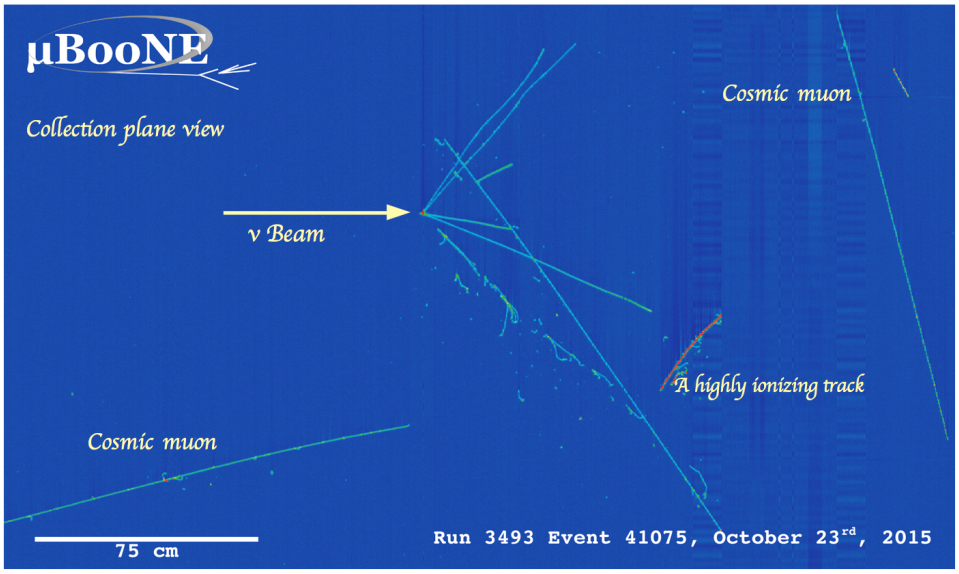


The horizontal axis represents the wires from collection plane, whereas vertical axis is the drift time from the position of the interaction until the charges being collected.
Source: (GOLLAPINNI, 2016).

# 4 NEUTRINO INTERACTIONS

In this section, the aim will be to describe a fundamental neutrino interaction as simple (and shortly) as possible through Fermi's Golden Rule and Feynman rules, giving at the end, the primordial physical entities of the neutrino interaction problem, putting it at the context of SBND.

First of all, what's interaction? The answer can be very complex depending on the context you are interested on, but human experience has a deep connection with gravitational effects. Even Isaac Newton was amazed with an answer: "[...] one body can act upon another at a distance, through a vacuum, [...] I believe no man who has in philosophical matters a competent faculty of thinking can ever fall into it" (AITCHISON; HEY, 2004). As Newton said, action at distance from one body to other can represent a kind of interaction meaning. Even when you touch your pen, or sit on the chair, no electron from your atoms touches the valence shell electron of those objects. Actually, it is done by a correspondent mediator boson to each fundamental interaction (shown on Table 2).

Table 2 – Fundamental forces and mediators[a]

| Mediator | Interaction | Coupling constant |
|---|---|---|
| $\gamma$ (photon) | Electromagnetic | $g_e = 0.302822$ |
| $g$ (gluon) | Strong | $g_s = 1.214$ |
| $W^{\pm}$ | Weak | $g_w = 0.6295$ |
| $Z^0$ | | $g_z = 0.7180$ |

[a] Gravitational interaction is not specified because of its quantum (theoretical) treatment is under discussion, as well as any experimental effort to a mediator detection is far from the current technology.
Source: author, using values from (GRIFFITHS, 2008).

Interactions are divided in two different phenomenon, being one related to *particle lifetime* and the other to *scattering*. The most important for this analysis is the second one, where the cross section is the invariant that gives the probability of , described by Fermi's theory in which golden rule is (GRIFFITHS, 2008)

$$\begin{aligned}\sigma = \quad & \frac{S}{4\sqrt{(p_1 \cdot p_2)^2 - (m_1 m_2)^2}} \int |\mathcal{M}|^2 (2\pi)^4 \\ & \delta^4(p_1 + p_2 - p_3 - ... - p_n) \prod_{i=3}^{n} \frac{d^3\boldsymbol{p}_i}{2\sqrt{\boldsymbol{p}_i^2 + m_i^2}(2\pi)^3}\end{aligned} \tag{21}$$

in which Dirac's delta ensures the energy conservation, all phase space of the outgoing particles is integrated, with $\mathcal{M}$ being the Feynman amplitude (or matrix element), which

carries the dynamical information and $S$ is a statistical factor, that corrects double counting of identical particles[7].

Sections 4.2 and 4.3 will be focused in solving the equation (21) for both Charged and Neutral Current, with $W^{\pm}$ and $Z^0$ as mediators respectively, in order to understand fundamental concepts of neutrino interactions for the muon neutrino-electron scattering in the process

$$\nu_\mu + e^- \rightarrow \nu_e + \mu^- \tag{22}$$

and

$$\nu_\mu + e^- \rightarrow \nu_\mu + e^- \tag{23}$$

Finally, a simple summary about neutrino-nucleus interaction will be described in Section 4.4, however we will discuss some essential concepts first.

## 4.1 DIRAC EQUATION

The goal now is introducing the Dirac equation showing the essential variables in the cross section calculation. A safe beginning is the energy conservation law

$$E = \frac{p^2}{2m} + V \ . \tag{24}$$

But a quantum treatment is required when such small scales as elementary particles are studied, so the energy and momentum can be interpreted as operators (LANDAU; LIFSHITZ, 1977)

$$\widehat{E} \equiv i\frac{\partial}{\partial t} \qquad\qquad \widehat{\boldsymbol{p}} \equiv i\boldsymbol{\nabla} \ , \tag{25}$$

and applied in (24). When the result is multiplied from right hand side by a generic ket $|\psi\rangle$,

$$i\frac{\partial}{\partial t}|\psi\rangle = -\frac{\nabla^2}{2m}|\psi\rangle + V|\psi\rangle \tag{26}$$

the Schrödinger equation comes up and becomes (6) using the Hamiltonian operator, in which is $\widehat{H} = -\frac{\nabla^2}{2m} + V$ (NAGASHIMA, 2010).

But equation (26) came from the classical concept of energy in terms of speed. In the scattering problem studied here, neutrinos are involved, those are almost (in a large spectrum) indistinguishable to the speed of light: they are truly relativistic entities

[7] Considering the (inelastic) scattering $a + b \rightarrow c + d + d + d + e + e$, the statistical factor will be $S = \frac{1}{3!}\frac{1}{2!} = \frac{1}{12}$.

(ANTONELLO et al., 2012). The consequence is that equation (26) is not valid at such situation. The theory of relativity bring new definitions of energy such as $E^2 = \boldsymbol{p}^2 + m^2$, but a more sophisticated way to get a relativistic version of (26) is using the 4-vector formalism, where the Lorentz invariant dot product is

$$p^\mu p_\mu = p^0 p^0 - p^1 p^1 - p^2 p^2 - p^3 p^3 = m^2 \ , \tag{27}$$

where considering the energy and momentum operators as in (25) (GRIFFITHS, 2008)

$$\widehat{p}_\mu \equiv i\partial_\mu \tag{28}$$

with derivatives being

$$\partial_0 = \frac{\partial}{\partial t} \qquad \partial_1 = \frac{\partial}{\partial x} \qquad \partial_2 = \frac{\partial}{\partial y} \qquad \partial_3 = \frac{\partial}{\partial z} \tag{29}$$

in Cartesian coordinates. Replacing (28) and (29) in (27) and multiplying by right hand by a wave function, it becomes

$$\frac{\partial^2}{\partial t^2} |\psi\rangle - \nabla^2 |\psi\rangle + m^2 |\psi\rangle = 0 \ , \tag{30}$$

where the D'Alambert operator (AITCHISON; HEY, 2004; NAGASHIMA, 2010)

$$\Box = \partial^\mu \partial_\mu = \frac{\partial^2}{\partial t^2} - \nabla^2 \ , \tag{31}$$

changes (30) to

$$(\Box + m^2) |\psi\rangle = 0 \ . \tag{32}$$

This is the Klein-Gordon equation, a relativistic approach of (26), but applied only for spin 0 particles, those do not represent most of known matter, including fermions, the group of particles treated here.

In order to develop an equation able to satisfy particles with half-integral spin, using the same initial proposal made in (27)

$$p^\mu p_\mu - m^2 = 0 \ , \tag{33}$$

Paul Dirac, in 1928, tried an approach using the distributive (GRIFFITHS, 2008)

$$p^\mu p_\mu - m^2 = (\gamma^j p_j + m)(\gamma^i p_i - m) = 0 \tag{34}$$

and forcing both of terms to be zero (GRIFFITHS, 2008), taking the second one and applying (28) for acting the result on a wave function from left-hand side

$$i\gamma^\mu \partial_\mu \Psi - m^2 \Psi = 0 \ , \tag{35}$$

which is Dirac equation. The parameter $\gamma^\mu$ is a set of $4 \times 4$ objects called Dirac's (or gamma) matrices, with values

$$\gamma^0 = \begin{pmatrix} \mathbb{1} & \mathbb{0} \\ \mathbb{0} & -\mathbb{1} \end{pmatrix} \qquad \gamma^a = \begin{pmatrix} \mathbb{0} & \boldsymbol{\sigma}_a \\ -\boldsymbol{\sigma}_a & \mathbb{0} \end{pmatrix} , \tag{36}$$

where zeros, units and sigmas[8] are $2 \times 2$ matrices. Therefore, $\Psi$ is a $4 \times 1$ dimension entity, that Dirac interpreted as a spinor (STEANE, 2013).

The plane waves solution for particles

$$\Psi(x) = ke^{-ip\cdot x}u_s(p) \tag{37}$$

and antiparticles

$$\Psi(x) = ke^{ip\cdot x}v_s(p) \ , \tag{38}$$

are able to describe fermions space-evolution, where $u_s(p)$ and $v_s(p)$ are Dirac Spinors with $s$ being the spin state. The relevant solutions for this scattering description are the particles going on the z-axis direction, such as[9] (AITCHISON; HEY, 2004)

$$u_{(1/2)} = \begin{pmatrix} \varepsilon \\ 0 \\ \dfrac{p_z}{\varepsilon} \\ \dfrac{p_x + ip_y}{\varepsilon} \end{pmatrix} \qquad u_{(-1/2)} = \begin{pmatrix} 0 \\ \varepsilon \\ \dfrac{p_x - ip_y}{\varepsilon} \\ \dfrac{-p_z}{\varepsilon} \end{pmatrix} \tag{39}$$

where $\varepsilon = \sqrt{E + m}$.

These results have remarkable importance, opening a window to Quantum Electrodynamics, one of the most precise theories in physics (HANNEKE; FOGWELL; GABRIELSE, 2008). The spinor solution will be essential to development of the next sections, since they are ingredients to the Feynman rules, a set of steps able to get the dynamical features of the scattering, whose description of terms is summarized in Table 3.

[8] $\boldsymbol{\sigma}_a$ represents Pauli matrices, with $a = (1, 2, 3)$.

[9] it is important to mention that $\Psi$ spinors are not Lorentz invariant, but the quantity $\bar{\Psi} = \Psi^\dagger\gamma^0$ is. It is called bilinear covariant and is needed to achieve the covariance of Dirac equation (GREINER, 2013).

Table 3 – Terms associated to Feynman rules for weak interactions

| Part of the diagram | Term |
|---|---|
| External lines (4-momenta) | $p_i$ |
| Internal lines (4-momenta) | $q_i$ |
| External lines (spinors) | $u$, $\bar{u}$ |
| Vertex ($W^{\pm}$) | $\frac{-ig_w}{2\sqrt{2}}\gamma^{\mu}(\mathbb{1}-\gamma^5)$ |
| ($Z^0$) | $\frac{-ig_z}{2}\gamma^{\mu}(c_V - c_A\gamma^5)$ |
| Propagators | $\frac{-i(g_{\mu\nu} - q_\mu q_\nu/M^2c^2)}{q^2 - M^2c^2}$ |
| Energy conservation | $(2\pi)^4\delta^4(k_1 + k_2 + ...)$ |
| Integrate over internal momenta | $\frac{d^4q}{(2\pi)^4}$ |
| Cancel the delta function | $(2\pi)^4\delta^4(p_1 + p_2 - ...)$ |

Source: author, using rules from (GRIFFITHS, 2008).

## 4.2 LEADING ORDER $\nu_\mu + e^-$ CHARGED CURRENT SCATTERING

The formulation of the scattering problem in SBND can start with the fact that the target is liquid argon, in which has obviously a density of electrons accompanying the atoms, where the consideration that can be taken is a scattering with an electron at rest at the detector frame description, which looks a good approximation for an extremely relativistic neutrino coming from the beam at energy around 700 MeV. Another simplification is considering the two-body scattering, that can be extended to a neutrino flux.

Figure 10 – Spatial orientation of a generic $\nu_\mu + e^-$ scattering where $l^-$ is the lepton generated and $\nu$ a neutrino

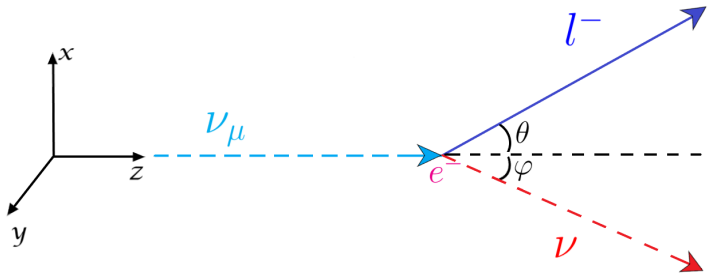


For charged current $l^- \equiv \mu^-$ and $\nu \equiv \nu_e$ and for neutral current $l^- \equiv e^-$ and $\nu \equiv \nu_\mu$. The measurable angle is $\theta$, between the incoming neutrino and outgoing charged lepton.
Source: author.

The Figure 10 shows a spatial representation of the scattering problem to be worked from now. The Feynman diagram in the Figure 11 shows the scattering described by (22), where an outgoing muon is the particle to be detected. The physical entity to be

calculated is the cross section, from equation (21), that in the lab frame will be

$$\sigma = \frac{1}{(8\pi)^2(p_e \cdot p_{\nu_\mu})} \int\int \begin{array}{l} |\mathcal{M}|^2 \delta\left(m_e + |\boldsymbol{p}_{\nu_\mu}| - |\boldsymbol{p}_{\nu_e}| - \sqrt{\boldsymbol{p}_\mu^2 + m_\mu^2}\right) \\ \delta^3(\boldsymbol{p}_{\nu_\mu} - \boldsymbol{p}_{\nu_e} - \boldsymbol{p}_\mu) \dfrac{d^3\boldsymbol{p}_{\nu_e} d^3\boldsymbol{p}_\mu}{|\boldsymbol{p}_{\nu_e}|\sqrt{\boldsymbol{p}_\mu^2 + m_\mu^2}} \end{array} . \tag{40}$$

One integral can be solved sending $\boldsymbol{p}_{\nu_e} \to \boldsymbol{p}_{\nu_\mu} - \boldsymbol{p}_\mu$ using the second delta function, as well as it is possible to use spherical coordinates making $d^3\boldsymbol{p}_\mu = |\boldsymbol{p}_\mu|^2 d|\boldsymbol{p}_\mu| d\Omega$, with $d\Omega$ being a solid angle, where $d\Omega = \sin\theta_\mu d\theta_\mu d\phi$. Hence,

$$\sigma = \frac{1}{(8\pi)^2 m_e |\boldsymbol{p}_{\nu_\mu}|} \int\int \begin{array}{l} |\mathcal{M}|^2 \delta\left(m_e + |\boldsymbol{p}_{\nu_\mu}| - |\boldsymbol{p}_{\nu_\mu} - \boldsymbol{p}_\mu| - \sqrt{\boldsymbol{p}_\mu^2 + m_\mu^2}\right) \\ \dfrac{|\boldsymbol{p}_\mu|^2 d|\boldsymbol{p}_\mu| d\Omega}{|\boldsymbol{p}_{\nu_\mu} - \boldsymbol{p}_\mu|\sqrt{\boldsymbol{p}_\mu^2 + m_\mu^2}} \end{array} , \tag{41}$$

where a change of variable as

$$r = |\boldsymbol{p}_{\nu_\mu} - \boldsymbol{p}_\mu| + \sqrt{\boldsymbol{p}_\mu^2 + m_\mu^2} \tag{42}$$

$$\frac{dr}{d|\boldsymbol{p}_\mu|} = \frac{|\boldsymbol{p}_\mu| - |\boldsymbol{p}_{\nu_\mu}|\cos\theta_\mu}{|\boldsymbol{p}_{\nu_\mu} - \boldsymbol{p}_\mu|} + \frac{|\boldsymbol{p}_\mu|}{\sqrt{\boldsymbol{p}_\mu^2 + m_\mu^2}} \tag{43}$$

$$\frac{dr}{d|\boldsymbol{p}_\mu|} = \frac{(|\boldsymbol{p}_\mu| - |\boldsymbol{p}_{\nu_\mu}|\cos\theta_\mu)\sqrt{\boldsymbol{p}_\mu^2 + m_\mu^2} + |\boldsymbol{p}_\mu||\boldsymbol{p}_{\nu_\mu} - \boldsymbol{p}_\mu|}{|\boldsymbol{p}_{\nu_\mu} - \boldsymbol{p}_\mu|\sqrt{\boldsymbol{p}_\mu^2 + m_\mu^2}} \tag{44}$$

$$\frac{dr}{d|\boldsymbol{p}_\mu|} = \frac{|\boldsymbol{p}_\mu|\left(r - \dfrac{|\boldsymbol{p}_{\nu_\mu}|}{|\boldsymbol{p}_\mu|}\sqrt{\boldsymbol{p}_\mu^2 + m_\mu^2}\cos\theta_\mu\right)}{|\boldsymbol{p}_{\nu_\mu} - \boldsymbol{p}_\mu|\sqrt{\boldsymbol{p}_\mu^2 + m_\mu^2}} \tag{45}$$

Figure 11 – Feynman Diagram for the neutrino interaction mediated by $W^\pm$ boson

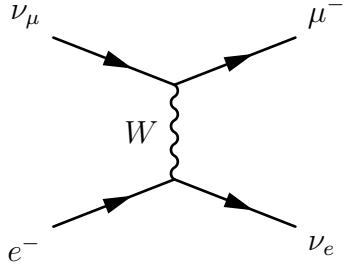


Source: author, adapted from (GRIFFITHS, 2008).

$$\frac{dr}{r - \frac{|\boldsymbol{p}_{\nu_\mu}|}{|\boldsymbol{p}_\mu|} E_\mu \cos\theta_\mu} = \frac{|\boldsymbol{p}_\mu| d|\boldsymbol{p}_\mu|}{|\boldsymbol{p}_{\nu_\mu} - \boldsymbol{p}_\mu| \sqrt{\boldsymbol{p}_\mu^2 + m_\mu^2}} \tag{46}$$

and replacing it in (41), using the fact that (LEO, 2012)

$$\sigma = \int \frac{d\sigma}{d\Omega} d\Omega \tag{47}$$

to get the differential cross section

$$\frac{d\sigma}{d\Omega} = \frac{1}{(8\pi)^2 m_e |\boldsymbol{p}_{\nu_\mu}|} \int |\mathcal{M}|^2 \delta\left(m_e + |\boldsymbol{p}_{\nu_\mu}| - r\right) \frac{|\boldsymbol{p}_\mu| dr}{r - \frac{|\boldsymbol{p}_{\nu_\mu}|}{|\boldsymbol{p}_\mu|} E_\mu \cos\theta_\mu} \tag{48}$$

where the delta function sends $r \to m_e + |\boldsymbol{p}_{\nu_\mu}|$, as

$$\frac{d\sigma_{CC}}{d\Omega} = \frac{|\mathcal{M}|^2 |\boldsymbol{p}_\mu|^2}{(8\pi)^2 m_e |\boldsymbol{p}_{\nu_\mu}| \left[m_e |\boldsymbol{p}_\mu| + |\boldsymbol{p}_{\nu_\mu}||\boldsymbol{p}_\mu| - |\boldsymbol{p}_{\nu_\mu}| E_\mu \cos\theta_\mu\right]} \tag{49}$$

which is a solution for differential cross section in the scattering described on Figures 10 and 11, that is proportional to momentum transferred to the muon. Even before solving the matrix element, it is possible suppress few dependencies starting to 3-momentum conservation

$$\boldsymbol{p}_{\nu_\mu} = \boldsymbol{p}_\mu + \boldsymbol{p}_{\nu_e} \tag{50}$$

$$\cos\theta_\mu = \frac{|\boldsymbol{p}_{\nu_\mu}|^2 + |\boldsymbol{p}_\mu|^2 - |\boldsymbol{p}_{\nu_e}|^2}{2|\boldsymbol{p}_{\nu_\mu}||\boldsymbol{p}_\mu|} \tag{51}$$

and in order to replace $|\boldsymbol{p}_{\nu_e}|$, the energy conservation

$$E_{\nu_\mu} + E_e = E_\mu + E_{\nu_e} \tag{52}$$

$$|\boldsymbol{p}_{\nu_e}| = |\boldsymbol{p}_{\nu_\mu}| + m_e - E_\mu \tag{53}$$

keeping a dependency only in the outgoing muon and incoming neutrino energy. It is important the mention that replacing (53) and (51) in (49), where an isotropic result is got, given the independence from direction. To access the dynamical information of this scattering, let's apply Feynman rules using Figure 11 in order to get the matrix element

$$\begin{aligned}\mathcal{M}_{CC} = \int \left\{\bar{\nu}_e \left[\frac{-ig_w}{2\sqrt{2}} \gamma^\alpha (\mathbb{1} - \gamma^5)\right] e\right\} \frac{-ig_{\mu\nu} - q_\mu q_\nu / M_W^2}{q^2 - M_W^2} \left\{\bar{\mu} \left[\frac{-ig_w}{2\sqrt{2}} \gamma^\nu (\mathbb{1} - \gamma^5)\right] \nu_\mu\right\} \\ (2\pi)^4 \delta^4(p_e - p_{\nu_e} - q)(2\pi)^4 \delta^4(q + p_{\nu_\mu} - p_\mu) \frac{d^4 q}{(2\pi)^4}\end{aligned} \tag{54}$$

where the particles symbols[10] are spinors and their respective covariants, $q$ is the 4-momentum transfer, $g_{\mu\nu}$ is the Minkowski metric, $M_W$ is the mass of the boson $W^{\pm}$ and $\gamma^5 = i\gamma^0\gamma^1\gamma^2\gamma^3$ (STEANE, 2013). The spectrum of SBND beam shows mostly of neutrino flux around 700 MeV, hence $q^2 \ll M_W^2$ (given the $M_W \approx 80$ GeV), what results in

$$\begin{aligned}\mathcal{M}_{CC} = \frac{-ig_w^2}{8M_W^2}\int \left\{\bar{\nu}_e\gamma^\alpha(\mathbb{1}-\gamma^5)e\right\}\left\{\bar{\mu}\gamma_\alpha(\mathbb{1}-\gamma^5)\nu_\mu\right\} \\ (2\pi)^4\delta^4(p_e - p_{\nu_e} - q)(2\pi)^4\delta^4(q + p_{\nu_\mu} - p_\mu)\frac{d^4q}{(2\pi)^4}\end{aligned} \tag{55}$$

where the solution is

$$\mathcal{M}_{CC} = \frac{g_w^2}{8M_W^2}\left\{\bar{\nu}_e\gamma^\alpha(\mathbb{1}-\gamma^5)e\right\}\left\{\bar{\mu}\gamma_\alpha(\mathbb{1}-\gamma^5)\nu_\mu\right\} . \tag{56}$$

But equation (49) shows that the quantity of interest is $|\mathcal{M}_{CC}|^2$, thus

$$\begin{aligned}|\mathcal{M}_{CC}|^2 = \mathcal{M}^\dagger\mathcal{M} = \frac{g_w^4}{64M_W^4}\left\{\bar{\nu}_e\gamma^\nu(\mathbb{1}-\gamma^5)e\right\}^\dagger\left\{\bar{\mu}\gamma_\nu(\mathbb{1}-\gamma^5)\nu_\mu\right\}^\dagger \\ \left\{\bar{\nu}_e\gamma^\alpha(\mathbb{1}-\gamma^5)e\right\}\left\{\bar{\mu}\gamma_\alpha(\mathbb{1}-\gamma^5)\nu_\mu\right\}\end{aligned} . \tag{57}$$

Taking the Hermitian from the first curly brackets

$$\begin{aligned}\left\{\bar{\nu}_e\gamma^\nu(\mathbb{1}-\gamma^5)e\right\}^\dagger = \left\{e^\dagger\mathbb{1}(\mathbb{1}-\gamma^5)\gamma^{\nu\dagger}\gamma^0\nu_e\right\} = \\ = \left\{e^\dagger\gamma^0\gamma^0(\mathbb{1}-\gamma^5)\gamma^{\nu\dagger}\gamma^0\nu_e\right\} = \left\{\bar{e}\gamma^0(\mathbb{1}-\gamma^5)\gamma^{\nu\dagger}\gamma^0\nu_e\right\}\end{aligned} , \tag{58}$$

where was used the fact that $\gamma^0\gamma^0 = \mathbb{1}$. The sandwich $\gamma^0(\mathbb{1}-\gamma^5)\gamma^{\nu\dagger}\gamma^0$ can be changed if using the anticommutation

$$\left\{\gamma^{\nu\dagger}, \gamma^5\right\} = 0 , \tag{59}$$

to get

$$\begin{aligned}\gamma^0(\mathbb{1}-\gamma^5)\gamma^{\nu\dagger}\gamma^0 = \gamma^0\gamma^{\nu\dagger}\gamma^0 - \gamma^0\gamma^5\gamma^{\nu\dagger}\gamma^0 = \gamma^0\gamma^{\nu\dagger}\gamma^0 + \gamma^5\gamma^0\gamma^{\nu\dagger}\gamma^0 = \\ = \gamma^\nu - \gamma^\nu\gamma^5 = \gamma^\nu(\mathbb{1}-\gamma^5)\end{aligned} \tag{60}$$

Making the same for the other Hermitian term in equation (57)

$$\left\{\bar{\mu}\gamma_\nu(\mathbb{1}-\gamma^5)\nu_\mu\right\}^\dagger = \left\{\bar{\nu}_\mu\gamma_\nu(\mathbb{1}-\gamma^5)\mu\right\} \tag{61}$$

[10] $\nu_\mu$, $e$, $\nu_e$ and $\mu$ and the covariant form as $\bar{\nu}_\mu$, $\bar{e}$, $\bar{\nu}_e$ and $\bar{\mu}$.

$$|\mathcal{M}_{CC}|^2 = \frac{g_w^4}{64M_W^4}\left\{\bar{\nu}_e\gamma^\alpha(\mathbb{1}-\gamma^5)e\right\}\left\{\bar{e}\gamma^\nu(\mathbb{1}-\gamma^5)\nu_e\right\} \\ \left\{\bar{\mu}\gamma_\alpha(\mathbb{1}-\gamma^5)\nu_\mu\right\}\left\{\bar{\nu}_\mu\gamma_\nu(\mathbb{1}-\gamma^5)\mu\right\} \quad . \tag{62}$$

To proceed, getting a consistent solution for $|\mathcal{M}_{CC}|^2$ it is important the mention that equation (39) reveals a spinors dependency of spin states, so how to get the correct spinor configuration? The answer for a beam as BNB is very simple: an average of the initial spins and sum of the final spin states (GRIFFITHS, 2008). Firstly, let's make the sum of final spins, letting the average to the end of the calculation, so

$$\sum_{spins}|\mathcal{M}_{CC}|^2 = \frac{g_w^4}{64M_W^4}\sum_{spins}^{(\nu_e,\mu)}\sum_{spins}^{(e,\nu_\mu)}\left\{\bar{\nu}_e\gamma^\alpha(\mathbb{1}-\gamma^5)e\right\}\left\{\bar{e}\gamma^\nu(\mathbb{1}-\gamma^5)\nu_e\right\} \\ \left\{\bar{\mu}\gamma_\alpha(\mathbb{1}-\gamma^5)\nu_\mu\right\}\left\{\bar{\nu}_\mu\gamma_\nu(\mathbb{1}-\gamma^5)\mu\right\} \tag{63}$$

and the completeness relation says (GRIFFITHS, 2008)

$$\sum_{spins} u\bar{u} = \gamma^\alpha p + \mathbb{m} \ , \tag{64}$$

can be applied in (63), where the mass $\mathbb{m} = \mathbb{1}m$ and $\mathbb{1}$ is $4\times 4$ unit matrix, therefore

$$\sum_{spins}|\mathcal{M}_{CC}|^2 = \frac{g_w^4}{64M_W^4}\sum_{spins}^{(\nu_e,\mu)}[\bar{\nu}_e\gamma^\alpha(\mathbb{1}-\gamma^5)(\not{p}_e+\mathbb{m}_e)\gamma^\nu(\mathbb{1}-\gamma^5)\nu_e] \\ [\bar{\mu}\gamma_\alpha(\mathbb{1}-\gamma^5)\not{p}_{\nu_\mu}\gamma_\nu(\mathbb{1}-\gamma^5)\mu] \tag{65}$$

where was considered the neutrino mass negligible and $\gamma^\alpha p = \not{p}$. Taking from equation (65) the shorthand

$$\xi_e = \gamma^\alpha(\mathbb{1}-\gamma^5)(\not{p}_e+\mathbb{m}_e)\gamma^\nu(\mathbb{1}-\gamma^5) \\ \xi_{\nu_\mu} = \gamma_\alpha(\mathbb{1}-\gamma^5)\not{p}_{\nu_\mu}\gamma_\nu(\mathbb{1}-\gamma^5) \tag{66}$$

thus

$$\sum_{spins}|\mathcal{M}_{CC}|^2 = \frac{g_w^4}{64M_W^4}\sum_{spins}^{(\nu_e,\mu)}[\bar{\nu}_e\xi_e\nu_e]\left[\bar{\mu}\xi_{\nu_\mu}\mu\right] \ . \tag{67}$$

The first bracket as well as the second one is cyclic if the matrix multiplication is done term by term (after all, they are just numbers)

$$\sum_{spins}^{(\nu_e,\mu)}\sum_{i,j=1}^{4}\bar{\nu}_e^i\xi_e^{ij}\nu_e^j = \sum_{spins}^{(\nu_e,\mu)}\sum_{i,j=1}^{4}\xi_e^{ij}\nu_e^j\bar{\nu}_e^i \tag{68}$$

therefore, applying (64), the result will be

$$\sum_{i,j=1}^{4} [\xi_e \not{p}_{\nu_e}]^{ii} = \mathrm{Tr}\Big(\xi_e \not{p}_{\nu_e}\Big) \ , \tag{69}$$

therefore, equation (67) will be

$$\begin{aligned}\sum_{spins} |\mathcal{M}_{CC}|^2 = \frac{g_w^4}{64 M_W^4} \mathrm{Tr}\Big[\gamma^\alpha(\mathbb{1}-\gamma^5)(\not{p}_e + \mathbb{m}_e)\gamma^\nu(\mathbb{1}-\gamma^5)\not{p}_{\nu_e}\Big] \\ \mathrm{Tr}\Big[\gamma_\alpha(\mathbb{1}-\gamma^5)\not{p}_{\nu_\mu}\gamma_\nu(\mathbb{1}-\gamma^5)(\not{p}_\mu + \mathbb{m}_\mu)\Big]\end{aligned} \tag{70}$$

where the combination of the last steps generating the trace were the Casimir's trick (GRIFFITHS, 2008).

Making the products and using the fact that $\mathrm{Tr}(A+B) = \mathrm{Tr}(A) + \mathrm{Tr}(B)$ and $\mathrm{Tr}(kA) = k\,\mathrm{Tr}(A)$ with $A$ and $B$ being matrices and $k$ a scalar, the traces in (70) changes to

$$\begin{aligned}&\Big[\mathrm{Tr}\Big(\gamma^\alpha \not{p}_e \gamma^\nu \not{p}_{\nu_e}\Big) + m_e \overset{0}{\cancel{\mathrm{Tr}}}(\gamma^\alpha\gamma^\nu \not{p}_{\nu_e}) - \mathrm{Tr}\Big(\gamma^\alpha\gamma^5 \not{p}_e \gamma^\nu \not{p}_{\nu_e}\Big) - \\ &m_e \overset{0}{\cancel{\mathrm{Tr}}}(\gamma^\alpha\gamma^5\gamma^\nu \not{p}_{\nu_e}) - \mathrm{Tr}\Big(\gamma^\alpha \not{p}_e \gamma^\nu\gamma^5 \not{p}_{\nu_e}\Big) - m_e \overset{0}{\cancel{\mathrm{Tr}}}(\gamma^\alpha\gamma^\nu\gamma^5 \not{p}_{\nu_e}) + \\ &\mathrm{Tr}\Big(\gamma^\alpha\gamma^5 \not{p}_e \gamma^\nu\gamma^5 \not{p}_{\nu_e}\Big) + m_e \overset{0}{\cancel{\mathrm{Tr}}}(\gamma^\alpha\gamma^5\gamma^\nu\gamma^5 \not{p}_{\nu_e})\Big]\Big[\mathrm{Tr}\Big(\gamma_\alpha \not{p}_{\nu_\mu}\gamma_\nu \not{p}_\mu\Big) - \\ &\mathrm{Tr}\Big(\gamma_\alpha \not{p}_{\nu_\mu}\gamma_\nu\gamma^5 \not{p}_\mu\Big) - \mathrm{Tr}\Big(\gamma_\alpha\gamma^5 \not{p}_{\nu_\mu}\gamma_\nu \not{p}_\mu\Big) + \mathrm{Tr}\Big(\gamma_\alpha\gamma^5 \not{p}_{\nu_\mu}\gamma_\nu\gamma^5 \not{p}_\mu\Big) + \\ &m_\mu \overset{0}{\cancel{\mathrm{Tr}}}(\gamma_\alpha \not{p}_{\nu_\mu}\gamma_\nu) - m_\mu \overset{0}{\cancel{\mathrm{Tr}}}(\gamma_\alpha \not{p}_{\nu_\mu}\gamma_\nu\gamma^5) - m_\mu \overset{0}{\cancel{\mathrm{Tr}}}(\gamma_\alpha\gamma^5 \not{p}_{\nu_\mu}\gamma_\nu) + \\ &m_\mu \overset{0}{\cancel{\mathrm{Tr}}}(\gamma_\alpha\gamma^5 \not{p}_{\nu_\mu}\gamma_\nu\gamma^5)\Big]\end{aligned} \tag{71}$$

where the null terms are due to the theorem: a trace of an odd number of gamma matrices is null[11] (LANCASTER; BLUNDELL, 2014). Applying the anticommutation relation for $\gamma^5$ from (59) and knowing that $\gamma^5\gamma^5 = \mathbb{1}$, (71) becomes

$$2\Big[\mathrm{Tr}\Big(\gamma^\alpha \not{p}_e \gamma^\nu \not{p}_{\nu_e}\Big) + \mathrm{Tr}\Big(\gamma^5\gamma^\alpha \not{p}_e \gamma^\nu \not{p}_{\nu_e}\Big)\Big]\Big[\mathrm{Tr}\Big(\gamma_\alpha \not{p}_{\nu_\mu}\gamma_\nu \not{p}_\mu\Big) + \mathrm{Tr}\Big(\gamma^5\gamma_\alpha \not{p}_{\nu_\mu}\gamma_\nu \not{p}_\mu\Big)\Big] \tag{72}$$

and the traces can be evaluated for the theorems (GRIFFITHS, 2008; LANCASTER; BLUNDELL, 2014)

$$\mathrm{Tr}\Big(\gamma^\alpha\gamma^\lambda\gamma^\nu\gamma^\tau\Big) = 4(g^{\alpha\lambda}g^{\nu\tau} - g^{\alpha\nu}g^{\lambda\tau} + g^{\alpha\tau}g^{\lambda\nu}) \tag{73}$$

[11] it is important the mention that $\gamma^5$ is a combination of 4 matrices, therefore the trace of the product of an odd number of gamma matrices by $\gamma^5$ will be zero too.

$$\mathrm{Tr}\Big(\gamma^5\gamma^\alpha\gamma^\lambda\gamma^\nu\gamma^\tau\Big) = 4i\epsilon^{\alpha\lambda\nu\tau}, \tag{74}$$

so

$$\begin{aligned} &64\left[p_e^\alpha p_{\nu_e}^\nu - g^{\alpha\nu}(p_e\cdot p_{\nu_e}) + p_e^\nu p_{\nu_e}^\alpha - i\epsilon^{\alpha\nu\lambda\tau}(p_e)_\lambda(p_{\nu_e})_\tau\right] \\ &\quad\left[(p_{\nu_\mu})_\alpha(p_\mu)_\nu - g_{\alpha\nu}(p_{\nu_\mu}\cdot p_\mu) + (p_{\nu_\mu})_\nu(p_\mu)_\alpha - i\epsilon_{\alpha\nu\kappa\rho}p_{\nu_\mu}^\kappa p_\mu^\rho\right] \end{aligned} \tag{75}$$

$$\begin{aligned} 64\Big[&4(p_e\cdot p_{\nu_\mu})(p_{\nu_e}\cdot p_\mu) - i\epsilon_{\alpha\nu\kappa\rho}p_{\nu_\mu}^\kappa p_\mu^\rho p_e^\alpha p_{\nu_e}^\nu - i\epsilon_{\alpha\nu\kappa\rho}p_{\nu_\mu}^\kappa p_\mu^\rho p_e^\nu p_{\nu_e}^\alpha - \\ &i\epsilon^{\alpha\nu\lambda\tau}(p_e)_\lambda(p_{\nu_e})_\tau(p_{\nu_\mu})_\alpha(p_\mu)_\nu - i\epsilon^{\alpha\nu\lambda\tau}(p_e)_\lambda(p_{\nu_e})_\tau(p_{\nu_\mu})_\nu(p_\mu)_\alpha + \\ &g^{\alpha\nu}(p_e\cdot p_{\nu_e})i\epsilon_{\alpha\nu\kappa\rho}p_{\nu_\mu}^\kappa p_\mu^\rho + g_{\alpha\nu}(p_{\nu_\mu}\cdot p_\mu)i\epsilon^{\alpha\nu\lambda\tau}(p_e)_\lambda(p_{\nu_e})_\tau\Big]. \end{aligned} \tag{76}$$

The two terms with superscript (as well as the two subscript) Levi-Civita tensors are antisymmetric, thus they cancel each other[12] and terms with Minkowski metric will be always null, since all $g^{\alpha\nu} = 0$ for $\alpha \neq \nu$ and all tensors $\epsilon_{\alpha\nu\kappa\rho} = 0$ when $\alpha = \nu$. Which remains is just

$$4^4(p_e\cdot p_{\nu_\mu})(p_{\nu_e}\cdot p_\mu) \tag{80}$$

resulting the Feynman amplitude, where was considered the average of the initial spin states[13] dividing the result by 2 ($-1/2$ and $1/2$), that in the lab frame (70) becomes

$$\left\langle|\mathcal{M}_{CC}|^2\right\rangle = 2\left(\frac{g_w}{M_W}\right)^4 m_e|\boldsymbol{p}_{\nu_\mu}|\;|\boldsymbol{p}_{\nu_e}|\left[E_\mu - |\boldsymbol{p}_\mu|\cos(\theta_\mu+\varphi)\right] \tag{81}$$

and $\varphi$ is the angle between the incoming and outgoing neutrino, which is undesirable, but the 4-momentum conservation gives

$$(p_{\nu_\mu} + p_e)^2 = (p_\mu + p_{\nu_e})^2 \tag{82}$$

[12] A way to demonstrate it is making

$$-i\epsilon_{\alpha\nu\kappa\rho}p_{\nu_\mu}^\kappa p_\mu^\rho p_e^\alpha p_{\nu_e}^\nu - i\epsilon_{\alpha\nu\kappa\rho}p_{\nu_\mu}^\kappa p_\mu^\rho p_e^\nu p_{\nu_e}^\alpha \tag{77}$$

and replacing $\alpha$ and $\nu$ at the last term, such as

$$-i\epsilon_{\alpha\nu\kappa\rho}p_{\nu_\mu}^\kappa p_\mu^\rho p_e^\alpha p_{\nu_e}^\nu - i\epsilon_{\nu\alpha\kappa\rho}p_{\nu_\mu}^\kappa p_\mu^\rho p_e^\alpha p_{\nu_e}^\nu \tag{78}$$

and replacing again only tensor indexes

$$-i\epsilon_{\alpha\nu\kappa\rho}p_{\nu_\mu}^\kappa p_\mu^\rho p_e^\alpha p_{\nu_e}^\nu + i\epsilon_{\alpha\nu\kappa\rho}p_{\nu_\mu}^\kappa p_\mu^\rho p_e^\alpha p_{\nu_e}^\nu = 0\ . \tag{79}$$

[13] Neutrinos are left handed, with only one spin configuration, but the electron has two of them.

$$m_e^2 + 2m_e|\boldsymbol{p}_{\nu_\mu}| = m_\mu^2 + 2E_\mu|\boldsymbol{p}_{\nu_e}| - 2|\boldsymbol{p}_\mu||\boldsymbol{p}_{\nu_e}|\cos(\theta_\mu + \varphi) \tag{83}$$

$$\frac{m_e^2 - m_\mu^2}{2} + m_e|\boldsymbol{p}_{\nu_\mu}| = |\boldsymbol{p}_{\nu_e}|\left[E_\mu - |\boldsymbol{p}_\mu|\cos(\theta_\mu + \varphi)\right] \tag{84}$$

that can be replaced in (81), simplifies to

$$\left\langle|\mathcal{M}_{CC}|^2\right\rangle = 2\left(\frac{g_w}{M_W}\right)^4 m_e^2 E_{\nu_\mu}^2\left(1 - \frac{m_\mu^2 - m_e^2}{2m_e E_{\nu_\mu}}\right) \tag{85}$$

where the neutrino energy came from the fact that $|\boldsymbol{p}_{\nu_\mu}| \equiv E_{\nu_\mu}$. Now, it is possible to get a total cross section, replacing (85) in (49) and integrating over the the solid angle, gives

$$\sigma_{CC} = \frac{8m_e G_F^2 E_{\nu_\mu}|\boldsymbol{p}_\mu|^3}{\pi K}\left(1 - \frac{m_\mu^2 - m_e^2}{2m_e E_{\nu_\mu}}\right) \tag{86}$$

$$K = 2m_e|\boldsymbol{p}_\mu|^2 + 2E_{\nu_\mu}|\boldsymbol{p}_\mu|^2 - E_\mu E_{\nu_\mu}^2 - E_\mu|\boldsymbol{p}_\mu|^2 + E_\mu\left(E_{\nu_\mu} + m_e - E_\mu\right)^2 \tag{87}$$

where were used the kinematic results from (51) and (53), getting a cumbersome but dependent only of $\nu_\mu$ and $\mu^-$ energies due to $|\boldsymbol{p}_\mu| = \sqrt{E_\mu^2 - m_\mu^2}$. The $G_F$ is the Fermi constant, coming from

$$\left(\frac{g_w}{M_W}\right)^4 = 32G_F^2\ . \tag{88}$$

Other representations as the differential related to the inelasticity parameter $y$ can be used in order to simplify the cross section to a function only of the neutrino energy

$$\frac{d\sigma_{CC}}{dy} = \frac{2m_e G_F^2 E_{\nu_\mu}}{\pi}\left(1 - \frac{m_\mu^2 - m_e^2}{2m_e E_{\nu_\mu}}\right) \tag{89}$$

where $y = (p_e \cdot q)/(p_e \cdot p_{\nu_\mu})$, that is a Lorentz invariant, which in this special case will be:

$$y = \frac{E_\mu}{E_{\nu_\mu}} - \frac{(m_\mu^2 + m_e^2)}{2m_e E_{\nu_\mu}} \tag{90}$$

considering the limits

$$0 < y < 1 - \frac{m_\mu^2}{2m_e E_{\nu_\mu} + m_e^2} \tag{91}$$

the integration gives the total cross section

$$\sigma_{CC} = \frac{2m_e G_F^2 E_{\nu_\mu}}{\pi}\left(1 - \frac{m_\mu^2 - m_e^2}{2m_e E_{\nu_\mu}}\right)\left(1 - \frac{m_\mu^2}{2m_e E_{\nu_\mu} + m_e^2}\right)\ . \tag{92}$$

For energy scales where $E_{\nu_\mu} \gg m_\mu^2$, (92) becomes

$$\sigma_{CC} \approx \frac{2m_e G_F^2 E_{\nu_\mu}}{\pi} \ . \tag{93}$$

The square of the sum the energy-momentum of initial particles gives the center of mass energy $s$

$$s = (p_{\nu_\mu} + p_e)^2 = m_e^2 + 2m_e E_{\nu_\mu} \approx 2m_e E_{\nu_\mu} \ , \tag{94}$$

changing (93) to

$$\sigma_{CC} \approx \frac{G_F^2 s}{\pi} \ . \tag{95}$$

This is a Lorentz invariant valid for high energies, but it is needed to look at the results very carefully. Starting to the kinetic requirements from the angular differential cross section in equation (49), in order to compare to (89) (in which has simpler analysis)

$$m_e|\boldsymbol{p}_\mu| + E_{\nu_\mu}|\boldsymbol{p}_\mu| > E_{\nu_\mu} E_\mu \cos\theta_\mu \ , \tag{96}$$

where in the limit case (where the outgoing muon is on the same direction of the incoming neutrino)

$$\cos\theta_\mu \to 1 \tag{97}$$

and (96) can be called as

$$\Delta_{CC} = m_e|\boldsymbol{p}_\mu| + E_{\nu_\mu}|\boldsymbol{p}_\mu| - E_{\nu_\mu} E_\mu \ . \tag{98}$$

Figure 12 shows colorful region with $\Delta_{CC} > 0$ and the red curve is the muon momentum when all neutrino energy goes to muon. The allowed region is, therefore, over the curve (where there is energy to the outgoing neutrino too) and in the colorful region (where $\Delta_{CC} > 0$, given the cross section assume only positive values), giving a threshold energy $\approx 11$ GeV which is out of the SBND spectrum shown in Figure 7: $\nu_\mu + e^-$ charge current scattering is not expected in the experiment. This fact can also be compared with equation (86), (89) and (92), where the terms in the bracket forces $E_{\nu_\mu} \geq (m_\mu^2 - m_e^2)/2m_e$, since cross section has to assume positive values, which has the same limit $E_{\nu_\mu} \approx 11$ GeV.

## 4.3 LEADING ORDER $\nu_\mu + e^-$ NEUTRAL CURRENT SCATTERING

For the neutral current, the simplification of an electron scattered at rest is valid as well, which Feynman diagram in Figure 13 shows the elastic scattering mediated by the $Z^0$ boson, where the system of coordinates are the same shown in Figure 10.

Figure 12 – CC energy threshold for $\nu_\mu + e^- \to \mu^- + \nu_e$ given by equation (98)

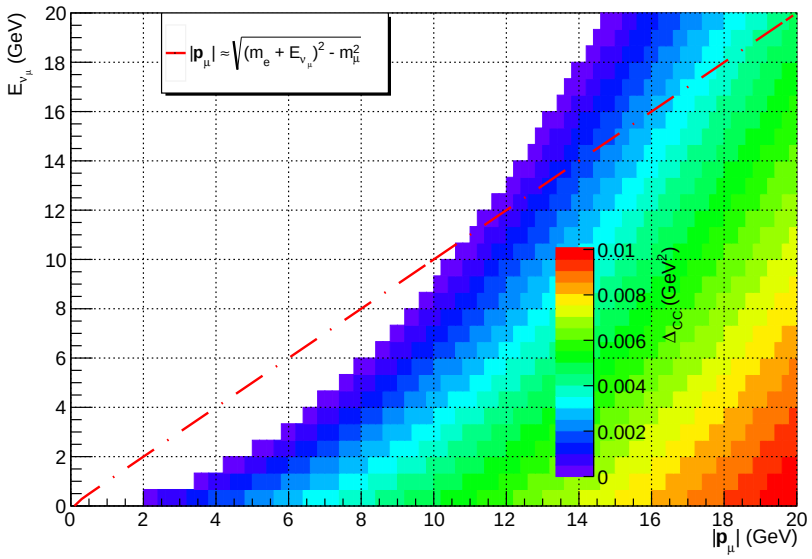


The red line shows the maximum values that absolute momentum of the outgoing muon can assume, considering the limit when $E_{\nu_e} \approx 0$, allowing only the region over the line (conservation of energy), whereas color region gives positive values of $\Delta_{CC}$. These assumptions show that values of $E_{\nu_\mu}$ under ~11 GeV are excluded. SBND will receive a beam with $\langle E_{\nu_\mu} \rangle \approx 700$ MeV, less than the required for this scattering.
Source: author.

The equivalent to equation (40) for the cross section will be

$$\sigma = \frac{1}{(8\pi)^2 (p_{\nu_\mu} \cdot p_e)} \int\int \; |\mathcal{M}|^2 \delta \left( m_e + |\boldsymbol{p}_{\nu_\mu}| - |\boldsymbol{p}'_{\nu_\mu}| - \sqrt{\boldsymbol{p}_e^{2'} + m_e^2} \right) \delta^3(\boldsymbol{p}_{\nu_\mu} - \boldsymbol{p}'_e - \boldsymbol{p}'_{\nu_\mu}) \frac{d^3\boldsymbol{p}'_{\nu_\mu} d^3\boldsymbol{p}'_e}{|\boldsymbol{p}'_{\nu_\mu}| \sqrt{\boldsymbol{p}_e^{2'} + m_e^2}} \; . \tag{99}$$

managing the terms with upper index (as $A'$) as the final state and without index ($A$) the initial state of the scattering. Solving (99) following similar steps shown since (41) until

Figure 13 – Feynman Diagram for the Neutral Current in the $\nu_\mu + e^-$ elastic scattering

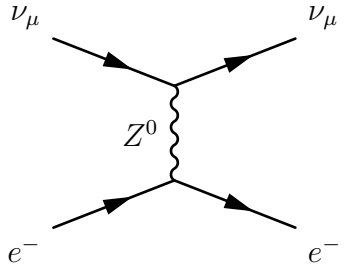


Source: author, adapted from (GRIFFITHS, 2008).

(49), differential cross section in the detector frame is given by

$$\frac{d\sigma_{NC}}{d\Omega} = \frac{|\mathcal{M}|^2 |\boldsymbol{p}_e^{'}|^2}{(8\pi)^2 |\boldsymbol{p}_{\nu_\mu}| m_e \left[ m_e |\boldsymbol{p}_e^{'}| + |\boldsymbol{p}_{\nu_\mu}||\boldsymbol{p}_e^{'}| - |\boldsymbol{p}_{\nu_\mu}| E_e^{'} \cos\theta_e \right]} \tag{100}$$

The angular dependency can be eliminated making the 3-momentum conservation

$$\boldsymbol{p}_{\nu_\mu} = \boldsymbol{p}_{\nu_\mu}^{'} + \boldsymbol{p}_e^{'} \tag{101}$$

$$\cos\theta_e = \frac{|\boldsymbol{p}_{\nu_\mu}|^2 + |\boldsymbol{p}_e^{'}|^2 - |\boldsymbol{p}_{\nu_\mu}^{'}|^2}{2|\boldsymbol{p}_{\nu_\mu}||\boldsymbol{p}_e^{'}|} \tag{102}$$

and the unmeasurable $|\boldsymbol{p}_{\nu_\mu}^{'}|$ is given by the energy conservation

$$E_{\nu_\mu} + E_e = E_{\nu_\mu}^{'} + E_e^{'} \tag{103}$$

$$|\boldsymbol{p}_{\nu_\mu}^{'}| = |\boldsymbol{p}_{\nu_\mu}| + m_e - E_e^{'} \tag{104}$$

Figure 14 – Total cross section for results of charged and neutral current $\nu_\mu + e^-$ scatterings for a large spectrum of energy

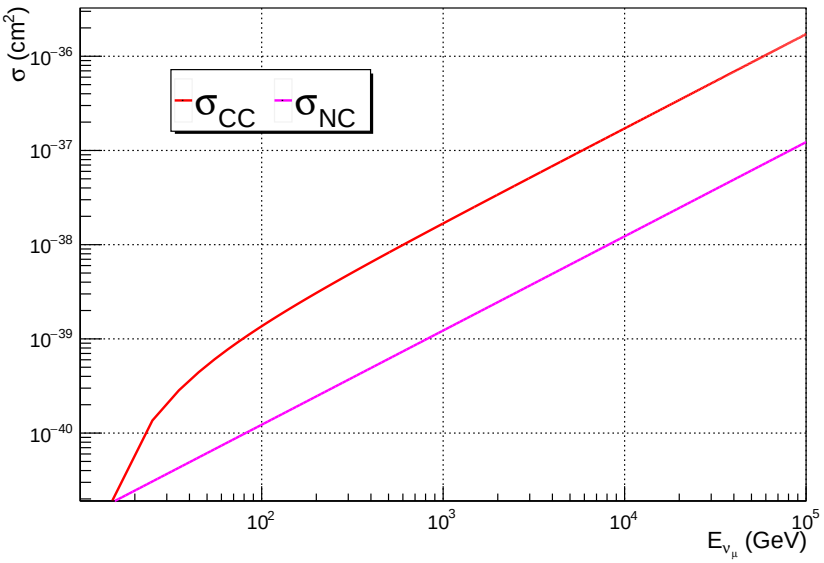


This graph is an extrapolation, given the scale of energy to be over the Z/W pole, as well as the simplification considering only the tree level
Source: author.

As in the CC case, only a function of the outgoing lepton energy, as well as the incoming neutrino energy.

Now, solving the matrix element applying Feynman rules in Figure 13,

$$\mathcal{M}_{NC} = \int \left\{ \bar{\nu}_{\mu}^{'} \left[ \frac{-ig_z}{2} \gamma^{\alpha} (\mathbb{1} - \gamma^5) \right] \nu_{\mu} \right\} \frac{-ig_{\mu\nu} - q_{\mu} q_{\nu} / M_Z^2}{q^2 - M_Z^2} \left\{ \bar{e}^{'} \left[ \frac{-ig_z}{2} \gamma^{\nu} (c_V - c_A \gamma^5) \right] e \right\} (2\pi)^4 \delta^4 (p_{\nu_{\mu}} - p_{\nu_{\mu}}^{'} - q)(2\pi)^4 \delta^4 (q + p_e - p_e^{'}) \frac{d^4 q}{(2\pi)^4} \tag{105}$$

with $c_A$ and $c_V$ being electron coupling coefficients of the neutral interaction those are specified as (GRIFFITHS, 2008)

$$\begin{aligned} c_A &= -\frac{1}{2} \\ c_V &= -\frac{1}{2} + 2\sin^2 \theta_w \end{aligned} \tag{106}$$

where the $\theta_w$ is the Weinberg angle and $\nu_{\mu}$ and $e$ are spinors of incoming particles and $\nu_{\mu}^{'}$ and $e^{'}$ the outgoing ones. With similar considerations adopted in (54) and (55), (105) becomes

$$\mathcal{M}_{NC} = \frac{g_z^2}{8 M_Z^2} \left\{ \bar{\nu}_{\mu}^{'} \gamma^{\alpha} (\mathbb{1} - \gamma^5) \nu_{\mu} \right\} \left\{ \bar{e}^{'} \gamma_{\alpha} (c_V - c_A \gamma^5) e \right\} \tag{107}$$

and the same set of tricks of the last section can be applied, giving

$$\begin{aligned} \left\langle |\mathcal{M}_{NC}|^2 \right\rangle = & \frac{1}{2} \left( \frac{g_z}{M_Z} \right)^4 \Big[ (c_V + c_A)^2 (p_{\nu_{\mu}} \cdot p_e)(p_{\nu_{\mu}}^{'} \cdot p_e^{'}) + \\ & (c_V - c_A)^2 (p_{\nu_{\mu}} \cdot p_e^{'})(p_e \cdot p_{\nu_{\mu}}^{'}) - m_e^2 (c_V^2 - c_A^2)(p_{\nu_{\mu}} \cdot p_e^{'}) \Big] \end{aligned} \tag{108}$$

that in the detector frame, according to representative parameters in the Figure 10, will be

$$\begin{aligned} \left\langle |\mathcal{M}_{NC}|^2 \right\rangle = & \frac{m_e |\boldsymbol{p}_{\nu_{\mu}}|}{2} \left( \frac{g_z}{M_Z} \right)^4 \Big\{ (c_V + c_A)^2 |\boldsymbol{p}_{\nu_{\mu}}^{'}| \left[ E_e^{'} - |\boldsymbol{p}_e^{'}| \cos(\theta_e + \varphi) \right] + \\ & (E_e^{'} - |\boldsymbol{p}_e^{'}| \cos\theta_e) \left[ (c_V - c_A)^2 |\boldsymbol{p}_{\nu_{\mu}}^{'}| - m_e (c_V^2 - c_A^2) \right] \Big\} \end{aligned} \tag{109}$$

whereas 4-momentum conservation can handle the $\varphi$ angle

$$(p_{\nu_{\mu}} + p_e)^2 = (p_{\nu_{\mu}}^{'} + p_e^{'})^2 \tag{110}$$

$$m_e^2 + 2 m_e |\boldsymbol{p}_{\nu_{\mu}}| = m_e^2 + 2 \left[ |\boldsymbol{p}_{\nu_{\mu}}^{'}| E_e^{'} - |\boldsymbol{p}_{\nu_{\mu}}^{'}| |\boldsymbol{p}_e^{'}| \cos(\theta_e + \varphi) \right] \tag{111}$$

Figure 15 – NC energy threshold for $\nu_\mu + e^- \to \nu_\mu + e^-$

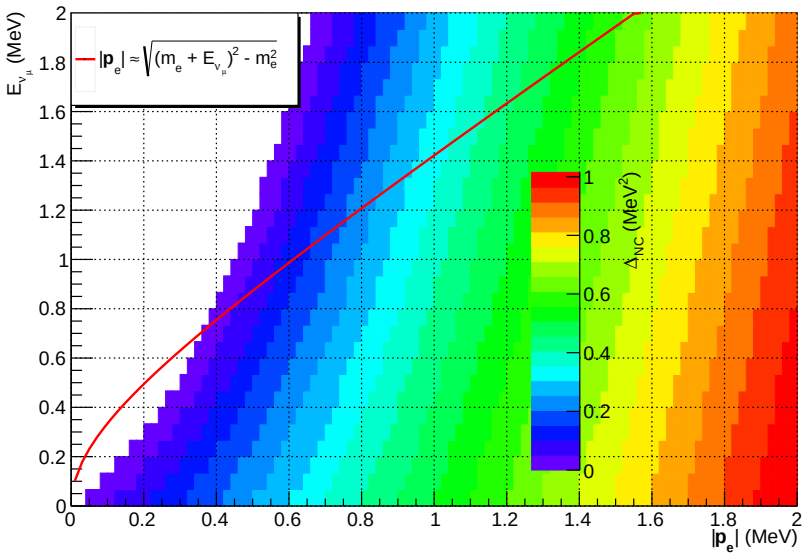


As in Figure 12, red line represents the maximum values for $|\boldsymbol{p_e}|$, considering $E'_{\nu_e} \approx 0$, so only the region colored over the line is allowed due the positive values of $\Delta_{NC}$, showing energies even $< 1$ MeV are kinematically possible, implying the existence of this elastic scattering in SBND due to the $\langle E_{\nu_\mu} \rangle \approx 700$ MeV of the beam.
Source: author.

$$m_e|\boldsymbol{p}_{\nu_\mu}| = |\boldsymbol{p}'_{\nu_\mu}| \left[E'_e - |\boldsymbol{p}'_e| \cos(\theta_e + \varphi)\right] \tag{112}$$

that can simplify the first term in the curly brackets of (109).

As in CC result, the differential cross section is isotropic, since the angular terms can be replaced for the solution obtained in (84), (102) and (104) and integrated over the solid angle, getting a total cross section as a function of the $E_{\nu_\mu}$ and $E'_e$, that won't be shown to avoid (unnecessary) a cumbersome notation, given the similarity to the results in the charged current scattering.

In comparison to CC, a similar condition have to be respected

$$m_e|\boldsymbol{p}'_e| + E_{\nu_\mu}|\boldsymbol{p}'_e| > E_{\nu_\mu} E'_e \cos\theta_e \tag{113}$$

thus, a parameter $\Delta_{NC}$ as

$$\Delta_{NC} = m_e|\boldsymbol{p}'_e| + E_{\nu_\mu}|\boldsymbol{p}'_e| - E_{\nu_\mu} E'_e \cos\theta_e \tag{114}$$

where in the case limit

$$|\boldsymbol{p}_e| \to \sqrt{E^2_{\nu_\mu} - m^2_e} \tag{115}$$

$$E_e \to E_{\nu_\mu} \tag{116}$$

and $\cos\theta_e \to 1$. Figure 15 shows that the NC scattering, differently of the CC case, can occur in SBND from even $\leq 1$ MeV. But the total cross section plotted on Figure 14 shows that its values are $\approx 10^{-41} cm^2$ for $E_{\nu_\mu} < 20$ GeV, which is the BNB range. Next section shows that neutrino-nucleus cross sections are approximately 2 or 3 orders of magnitude greater than this.

## 4.4 NEUTRINO-NUCLEUS SCATTERING

The neutrino-nucleus cross section is higher than the neutrino-lepton studied before, being now a composite, much more complicated entity and it is going to be the dominant interaction way in SBND (ANTONELLO et al., 2015). But a huge problem arises from nuclear physics: the neutrino-nucleus scattering is a source of different processes with dependency to the neutrino energy. It turns out that different models are needed to describe the whole picture and can be separated into three main processes:

- QES (Quasi-Elastic (and elastic) Scattering): the neutrino interacts to a nucleon generating a charged lepton and a nucleon in charged and neutral current ($\sim< 2$ GeV, $\nu_\mu + N \to \mu^- + N'$). It is the predominant process for few GeV scatterings and will be the main interaction in SBND.

Figure 16 – Feynman diagrams for QES

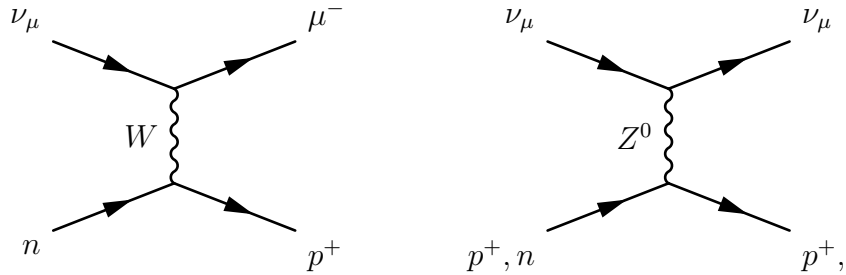


(a) QES in charged current interaction. (b) QES in neutral current interaction.

In (b) the same nucleon that goes in, goes out. Only the muon neutrino was described, since it will be the only flavor with importance in this study due to the BNB composition shown in Figure 7 (FORMAGGIO; ZELLER, 2012).
Source: author, adapted from (FORMAGGIO; ZELLER, 2012).

- RES (RESonance production): the neutrino excites the nucleon, creating an baryonic resonance, decaying into mesons ($\sim 0.5-100$ GeV, $\nu_\mu + N \to \mu^- + \Delta \to \mu^- + \pi + N'$);

  Also the pion production can happen coherently, in which the neutrino scatters off the nucleus and a forward pion is present in the final state ($\nu_\mu + Ar \to \nu_\mu + Ar + \pi^0$ or $\nu_\mu + Ar \to \mu^- + Ar + \pi^+$) (FORMAGGIO; ZELLER, 2012).

- DIS (Deep Inelastic Scattering): at high energies ($\sim>$ 20 GeV) the neutrino wave length is shorter than nucleons, generating hadronic systems in the final state

Figure 17 – Feynman diagrams for RES

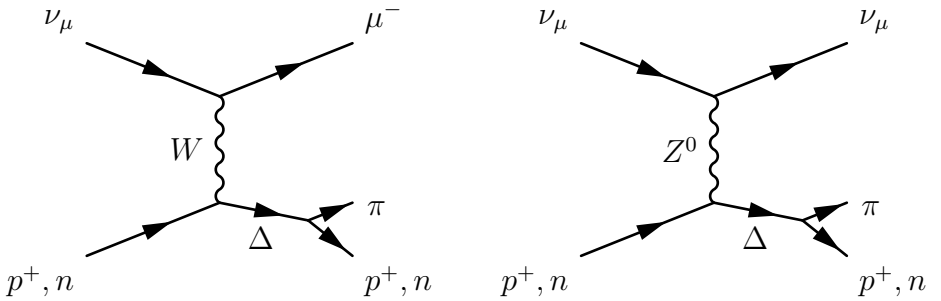


(a) RES in charged current interaction. (b) RES in neutral current interaction.

The $\Delta$ resonance has different possibilities of charges, resulting in $\pi^0$, $\pi^+$ and $\pi^-$ in the final state for $\nu_\mu$ scatterings.
Source: author, adapted from (FORMAGGIO; ZELLER, 2012; PARTYKA, 2013).

($\nu_\mu + Q \rightarrow \mu^- + H$ or $\nu_\mu + Q \rightarrow \nu_\mu + H$) (FORMAGGIO; ZELLER, 2012; PALAMARA, 2013).

Only the two first are relevant to SBND, because of the beam spectrum shown in Figure 7. The neutrino cross section for these three processes are described in Figure 18, showing the difficult description in low energy interactions, due the number of different processes.

In addition, the final state interactions (FSI), which are effects provided by re-interactions of secondary particles to nucleons before exiting the nucleus, have also huge impact in neutrino-nucleus scattering due to the disagreement amongst models interfering in multiplicities as well (PARTYKA, 2013; FORMAGGIO; ZELLER, 2012; PALAMARA, 2013).

The multiplicity[14] (M) expected in SBND, which at BNB energies is $\approx 80\%$ for $M = 2$ (from QES, $\nu_\mu n \rightarrow \mu^- p^+$, from neutral pion production with RES, $\nu_\mu n \rightarrow \Delta^+ \mu^- \rightarrow \mu^- p^+ \pi^0$ and from coherent pion production, $\nu_\mu Ar \rightarrow \mu^- \pi^+ Ar$), $\approx 20\%$ for $M = 3$ (from RES, $\nu_\mu p^+ \rightarrow \mu^- \Delta^{++} \rightarrow \mu^- p^+ \pi^+$) and $\approx 1\%$ for $M > 3$ (basically produced from DIS) (ADAMS et al., 2018; ALKIN, 2017), can also be affected by FSI.

This study won't be able to describe deeply neutrino-nucleus interaction phenomena, which can be more explored in the review of Formaggio and Zeller (2012) for an interested reader. Instead the analysis will make use of GENIE, which is the main event generator for neutrino interaction studies and consists in putting together the most relevant models for each range of energy in order to simulate the interaction on specific targets (argon in the case of LArTPCs).

GENIE uses Llewellyn-Smith model for CC QES (ANDREOPOULOS et al., 2015; SMITH, 1971) and the model described by Ahrens et al. for NC QES (ANDREOPOULOS

[14] At this context, it means a number of primary charged particles produced in a scattering at the final state.

Figure 18 – Neutrino-nucleus cross section in different processes in a spectrum

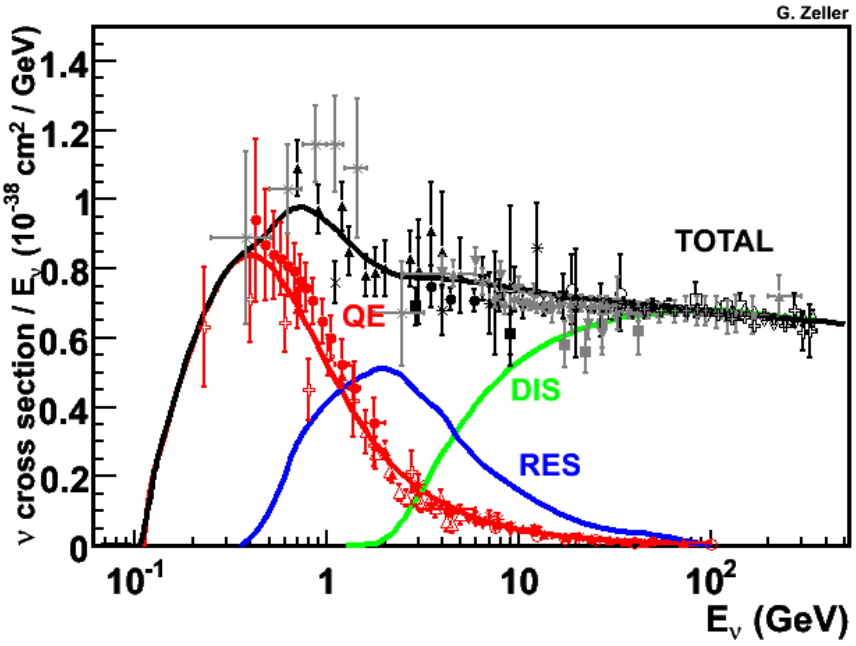


The lines were plotted using NUANCE event generator.
Source: (FORMAGGIO; ZELLER, 2012).

et al., 2015; AHRENS et al., 1987), whereas RES (as well as the coherent scattering) is described by Rein-Sehgal model (ANDREOPOULOS et al., 2015; REIN; SEHGAL, 1981; REIN; SEHGAL, 1983). DIS is calculated using Bodek and Yang model (ANDREOPOULOS et al., 2015; BODEK; YANG, 2003). Next section will describe the context that GENIE is introduced in a simulation.

# 5 SIMULATED DATA ANALYSIS

Figure 19 – Simulation process of LArTPC experiments managed by LArSoft framework

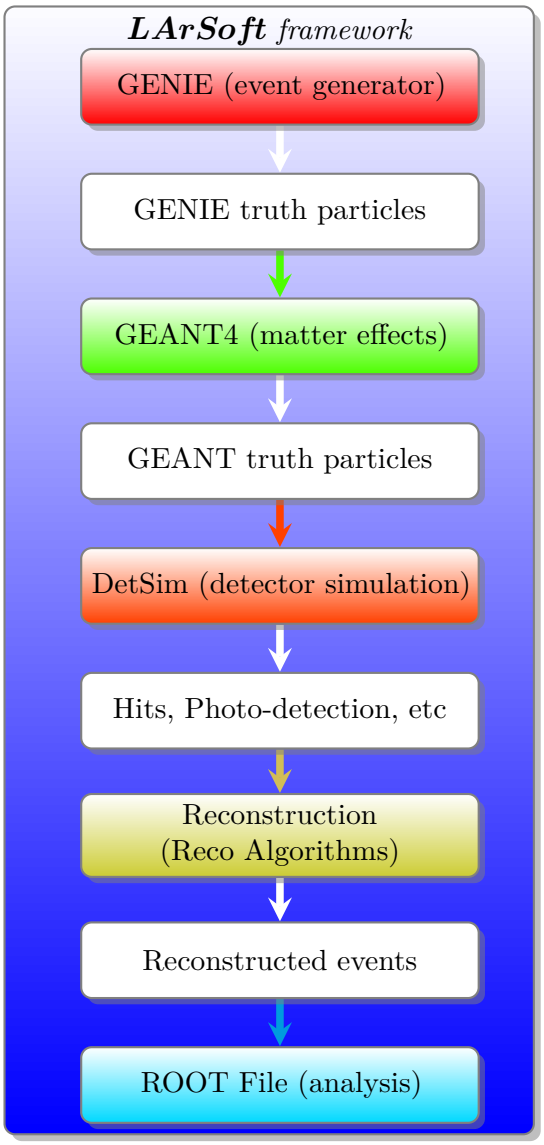


White boxes represent the output information for each step resulting at the end in ROOT files. The beam is not the only possible flux, that can come from cosmic rays, where the tool able to simulate it is called CORSIKA, that is not exclusive for neutrino physics (WENTZ et al., 2003).
Source: author.

How can the data from a particle detector to be compared to expected for Standard Model? Results are generally detector dependent, as well as flux dependent and can depend of the choice of a model. A way around of these challenges is the Monte Carlo (MC) simulation, which are statistical techniques of random numbers in order understand behavior of probabilistic phenomena, strongly connected to computational tools, that in

the context of particle detection, joins all geometrical and physical information, generating predictions of essential matters to detector strategy and design from simulation.

SBND uses powerful tools, starting to GENIE as event generator, that can describe neutrino-argon interactions for the specific detector geometry (ANDREOPOULOS et al., 2015), giving the final state particles to GEANT4, which is able to simulate the resulting particles passing through the matter (GEANT et al., 2012). This information is able to generate a detector simulation, consisting in applying electronics effects, depending of each detector. The results are information enough to try to reconstruct simulated events from the detector response. All of these steps are managed by LArSoft, a common software for liquid argon detectors (CHURCH, 2013; ANTONELLO et al., 2015; PARTYKA, 2013), on the other hand uses ART a framework that joins an infinity of tools for simulation approach. The details of each tool can be found in (ANDREOPOULOS et al., 2015) (GENIE), (GEANT et al., 2012) (GEANT4), (CHURCH, 2013) (LArSoft) and (GREEN et al., 2012) (ART). Figure 19 shows a simplified process of event simulation. The combination of those steps generates ROOT files in a Tree format which numerous informations are addressed in the ***truth*** level, composed by a combination of GENIE and GEANT4 simulated data, that is the predicted behavior from the $\nu$-Ar models, as well as the information for ***reconstruction***, that simulates the detector interpretation capabilities for the perturbations created by the neutrino interaction. In a LArTPC the fundamental perturbation is the hit, which means the charge deposition in wire planes, where the combination of them from the same event can give all information regarding calorimetry (amount of energy of detected particle) and directionality, providing a 3D reconstruction.

The simulation process using LArSoft allows to use BNB specifications to create events inside the detector geometry, with secondary particles interacting to argon, leaving charges and radiation. All of these physical processes are included in a high confidence level to expected in reality. This section will discuss, topologically, a MC simulation of 50,000 events made by SBND production team using LArSoft framework, composed by only one neutrino interaction per event, in a total of $8.05 \times 10^{15}$ POT, in other words, letting go the dynamics of weak interactions studied until now, to see their results inside the detector. The goal is very simple: to look at the responses of different particles in the final states with and without a pion, and if possible, to see calorimetric features of each one and at the end, select three of them: muon, pion and proton. To achieve it, a set of ROOT files containing simulated data were merged and the resulting file was analyzed with a macro written in C++ language, able to extract all relevant information, looping over each event of the ROOT Tree.

The strategy is using truth information to see simulated behavior in Section 5.1 and after that, to look at the detector simulation and track reconstruction in Section 5.2. It will allow to use the simulated data to perform cuts, those can be used in a simple particle identification exercise in CC 0 and 1 $\pi^{\pm}$.

## 5.1 TRUTH DISTRIBUTIONS

Figure 20 – Spectrum distribution in the MC production

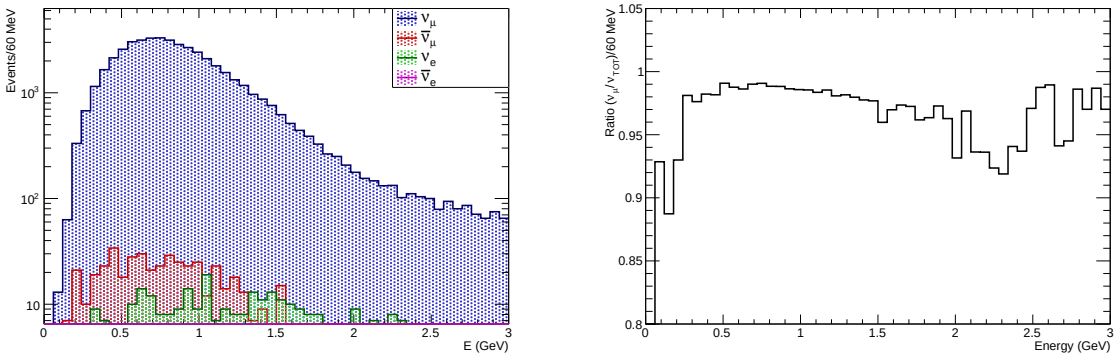


(a) Simulated spectrum of neutrinos those interacted in the LArTPC. The number of events caused by flavors different of $\nu_\mu$ is very low proportionally.

(b) Ratio of the number of simulated $\nu_\mu$ interactions. Around ≈1 GeV is concentrated the most of events, where is the expected peak of $\nu_\mu$ in BNB.

Source: author.

First of all, the truth neutrino interactions in a spectrum of the sample, in different flavors, is shown in Figure 20a, whereas Figure 20b provides the predominance of $\nu_\mu$ interactions, given the expected flux shown in Figure 7. But this result contemplates all interactions from truth information. This analysis is more specific, where only $\nu_\mu$ charged

Figure 21 – Muon momentum distribution for CC 0 and 1 pion events

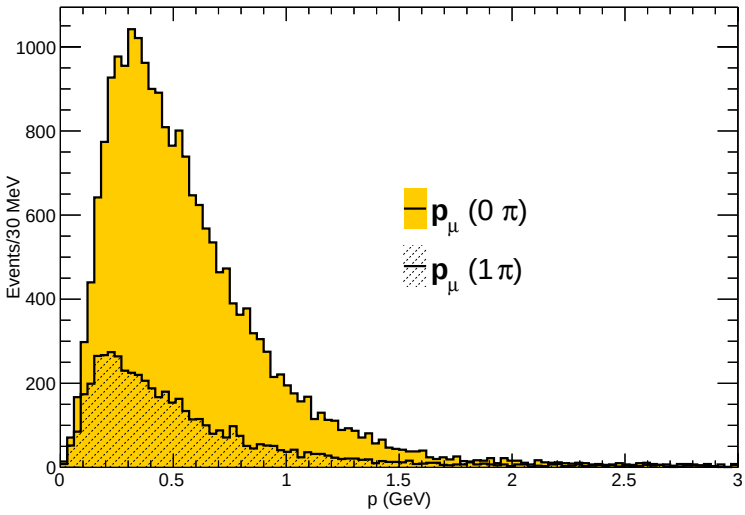


The spectrum distribution follows the flux behavior described in Figure 20, but the peak for 1 $\pi$ histogram is shifted to lower energies, indicating a influence of the different scattering process and the partition of energy between muon and pion.
Source: author.

Figure 22 – Spectrum of MC $\mu^-$, $\pi^\pm$ and $p^+$ of CC 0 (a) and 1 (b) $\pi$ topologies

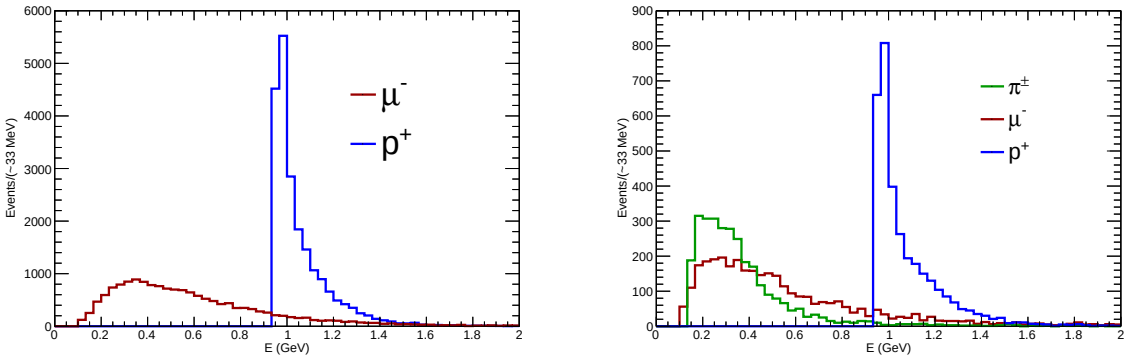


(a) CC0$\pi$ (b) CC1$\pi$

The proton distribution is very sharp around 1 GeV, whereas muon and pion have less energetic distribution and larger range. Only GEANT particles were attempt, with a required 3 mm track, that is the distance between wires in the detector.
Source: author.

Figure 23 – Proton multiplicity for CC 0 and 1 $\pi^\pm$ events

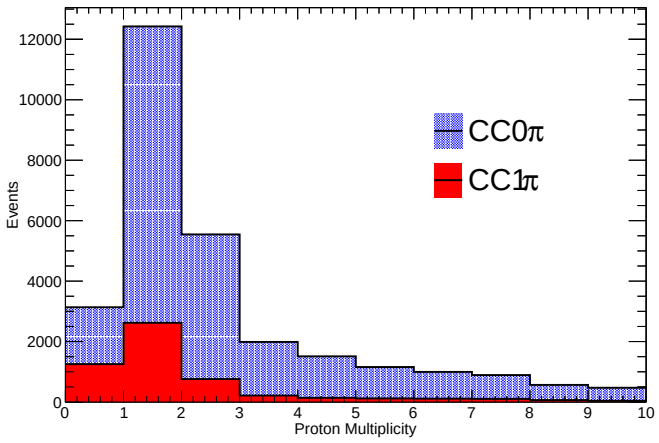


It is evident that the range 0-3 is the most frequent.
Source: author.

current events are interesting and a muon is generated at the final state. But specifying even more, let's look only events with and without one pion, created by the RES process, or even by QES with final state interactions. Figure 21 shows the muon spectrum for either 0 and 1 pion in the final state. The distribution has the flux behavior shown in 20, but for spectrum coming from CC1$\pi$, the most probable value is shifted to the left, indicating the magnitude of partition of energy between the muon and pion.

These two topologies are obviously, distinguishable by the presence of a pion. But neutrons and protons can be generated, being the neutron a big problem that won't be discussed here, given the neutral charge and its decay providing miss-identification in

Figure 24 – Muon and pion distribution of momentum and angle for CC1$\pi$ events

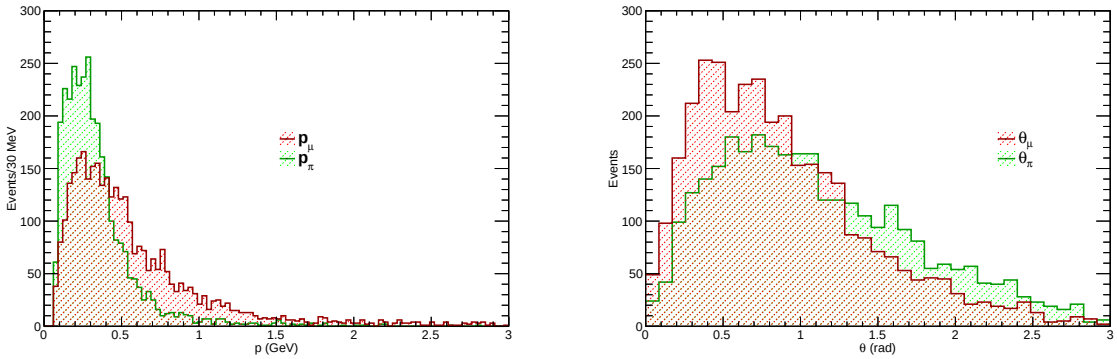


(a) Momentum (b) Scattering angle

It was required a GEANT track length $> 2$ cm.
Source: author.

any point of the detector. At this context, Figure 22 shows the spectrum of $\mu^-$, $\pi^\pm$ and $p^+$ considering all CC 0 and 1 $\pi^\pm$ events, showing that protons to be detected, are in general, more energetic than muons and pions and in higher number. it is explained by the possibility of proton multiplicity, or more than one proton created by a neutrino-nucleus scattering, that is plotted in Figure 23, and reaffirm this hypothesis. An important aspect of the distribution in Figure 22 is the similarity of muon and pion, realizing a possible miss-identification in terms of energy: what would be a feature to distinguish them? Figure 24 takes momentum and scattering angle from events with both a pion and a muon (CC1$\pi$), but the results are very similar, since the histograms are superimposed. Another approach is getting the length of GEANT track and the distributions are in Figure 25. For CC1$\pi$ events and considering all events, the muon track is in general larger than the pion.

Figure 25 – Track length distribution of muon, pion and proton for CC1$\pi$ events and all CC events

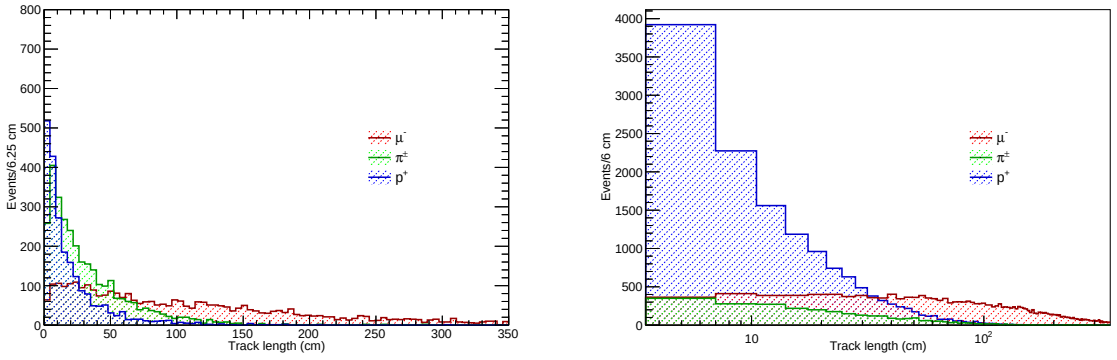


(a) CC1$\pi$ (b) All events

It was required a GEANT track length $> 2$ cm.
Source: author.

Next section will explore some of this features, including the calorimetric information, but now from detector simulation and reconstruction, where the response is less obvious, but much more relevant in the sense of developing techniques to recognize particles and topologies.

## 5.2 DETECTOR SIMULATION

Figure 26 – 3D view of the SBND geometry with an neutrino event

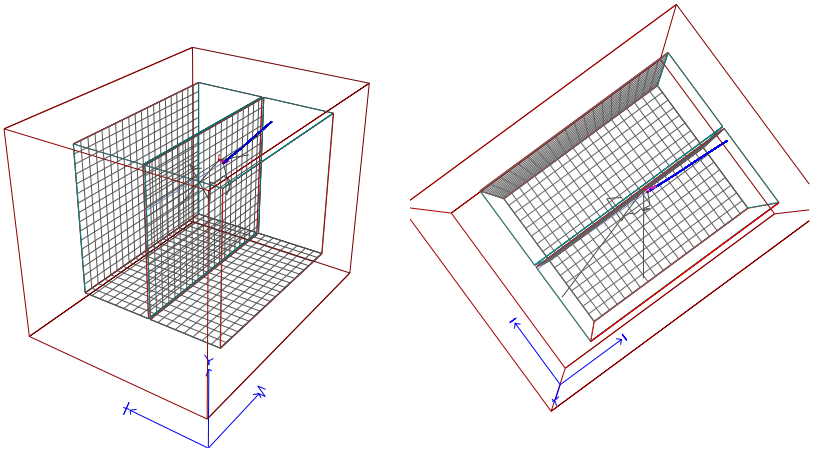

Both truth and reconstructed muon track (in blue) are shown. The beam goes trough XY plane to at positive direction Z, being a diagonal (left) and top (right) perspective of the event. The wire chambers are on the left an at the middle. Grey lines around interaction vertex (in pink) correspond to neutrons, those can't be directly detect, due its neutral charge.
Source: author.

Figure 26 reveals the detector geometry, developed in GEANT4, with a neutrino event with a very forward muon (blue) and a short pion track (pink), reconstructed by LArSoft with a projection matching algorithm (PMA). The gray tracks are from a neutron re-scattering many times in the detector. The event display picture shown in Figure 27a gives the same event, with reconstructed tracks and the axis are time × wires × charge for the three planes of the detector. Another way to see this event is a complete spatial display, shown in Figure 27b. All of this information comes from detector simulation and reconstruction steps shown in Figure 19.

A particle identification study can be made in many ways, but a very particular feature of particles those interact electromagnetically in any material medium is their loss energy along space, with finger print described by Bethe-Bloch equation, which is shown in Figure 28. So, to see the calorimetric capability of the detector considering the loss energy along space, Figure 29 shows $-dE/dx$ × energy × number of hits. The Bethe-Bloch curves provides $p^+$, $\mu^-$, $\pi^\pm$ and $e^-$ manifestations in the data, what reveals the possibility

Figure 27 – Display of a CC event in wire planes view (a) and geometric view (b)

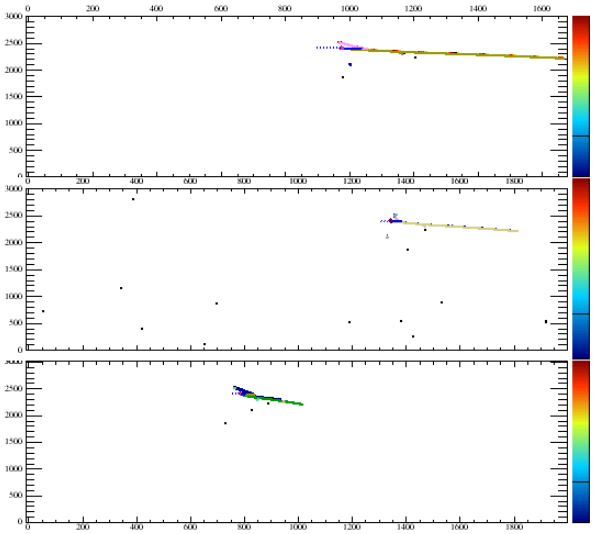

(a) Display of simulated event shown in Figure 26. X axis represents the wire numbers and Y axis is time of drift of charges and Z axis is the deposited charge. Considering a velocity of drift, the track shown is top view of the detector. Top window represents the collection plane and others are induction planes of wires.

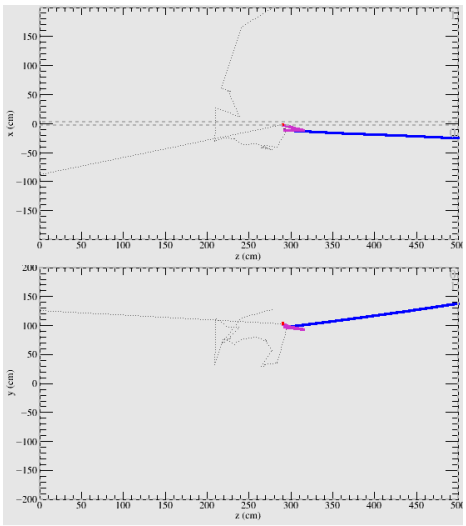

(b) Geometrical event of XZ and YZ planes. Doted gray lines show neutrons those can't be detected and comes from truth information. The colored track comes from reconstruction algorithms.

Source: author.

of a determined particle into many events, which is not much refined approach. But how to look at event by event and see differences those allows a particle recognizing?

First, a look in each topology and individual particles from reconstructed tracks can provide more information about energy loss and are shown in Figure 30, where a Landau distribution was used to see that the $\sigma$ of particles are slightly different between pion and muon, but hugely different in the case of the proton for normalized histograms, as well as the peak is very distinguishable among each one.

All this information provides some features:

- Figure 22 shows that generated protons have energy average greater that the muon and pion in both topologies (CC0$\pi$ and CC1$\pi$), as well as they are in higher number as shown in Figure 23;

- Figure 25 shows that the order of average of track length is muon - pion - proton;

- The order of peak magnitude of the normalized Landau distribution is muon - pion - proton, which is probably connected to the length of the track, with the muon as a minimum ionizing particle;

Figure 28 – Bethe-Bloch equation for different particles in argon

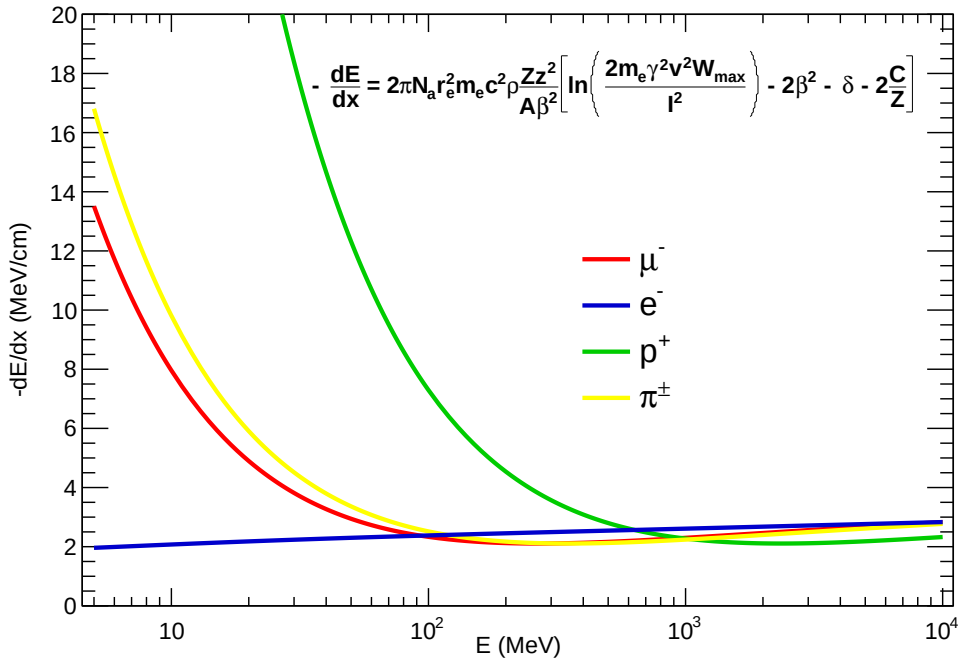


$N_a$ is Avogadro's number, $r_e$ is the classical electron radius, $m_e$ is the electron mass, $c$ the speed of light, $\rho$, $Z$ and is the density and atomic number of the medium, $\beta = v/c$, $\gamma = 1/\sqrt{(1-\beta^2)}$, $z$ and $v$ are charge and speed of the incident particle, $I$ is the mean excitation potential, $W_{max}$ is the maximum energy transfer in a single collision, being $W_{max} = 2m_e c^2\beta^2\gamma^2/(1 + 2m_e M^{-1}\sqrt{1+\beta^2\gamma^2} + m_e^2 M^{-2})$. $\delta$ and $C$ are correction factors. This effect is a powerful particle identification. Equation taken from (LEO, 2012).
Source: author, adapted from (LUZIO, 2016).

- As much as the peak is higher, the width ($\sigma$) is larger, what is expected. This remarks that the proton reaches, in general, higher values of $-dE/dx$;

The proposal is to use these results in a simple set of assumptions able to make a selection tool, with limited efficiency, used for CC events, only for muon, charged pion and proton recognizing, setting 2 as a maximum number of tracks. Thus:

- Only a track $> 2$ cm is considered;
- If only one track was reconstructed, it is a muon;
- When 2 tracks were reconstructed, the track with higher length is a muon;
- Fitting each track of each event with a Landau distribution, as shown in the event of Figure 31, it is possible to use parameters from a Landau fit over 5000 CC events with less than three tracks reconstructed in order to separate pions and protons. Using 3 Landau parameters (MPV - Most Probable Value, $\sigma$, height), it is possible to choose parameters ranges for each particle.

Figure 29 – Energy loss for CC events for CC0$\pi$, CC1$\pi$ and all events in two range of energies

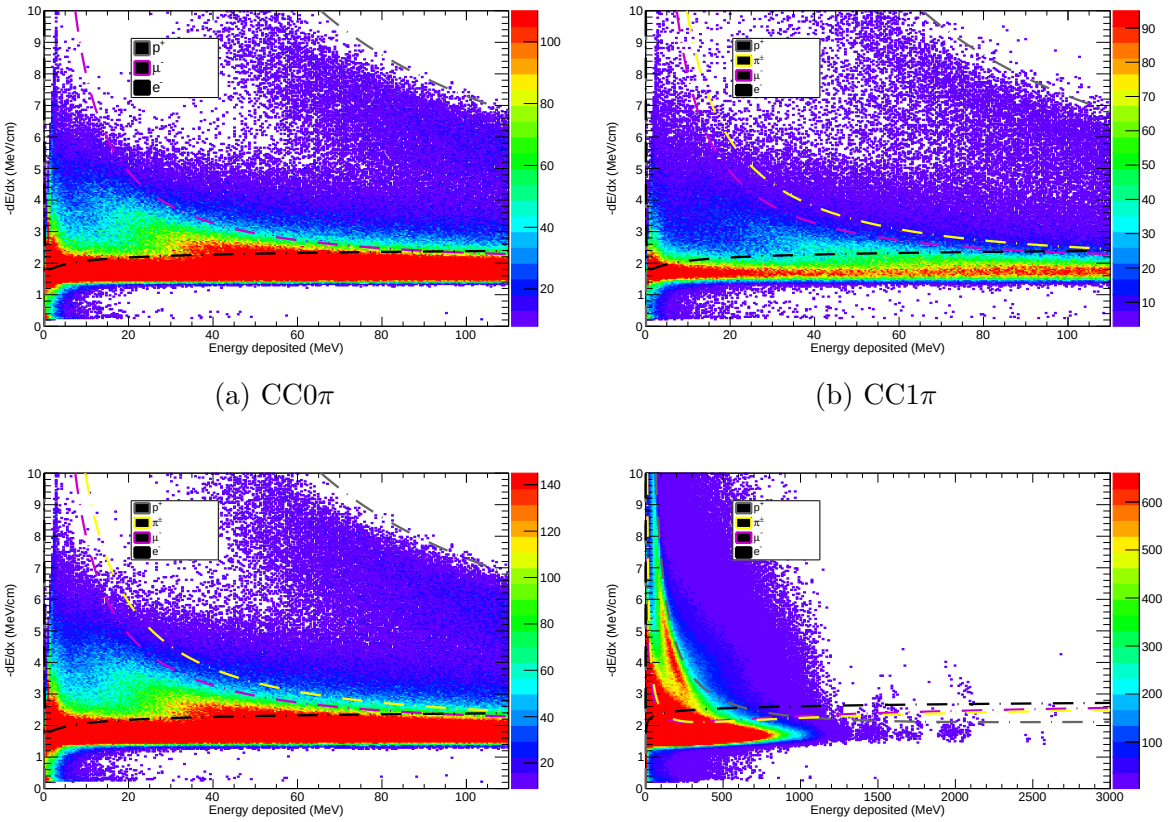


(a) CC0$\pi$ (b) CC1$\pi$

(c) CC all events (d) CC all events 0-3 GeV

The lines plotted are from Bethe-Bloch equation for proton, muon, pion and electron. There is a visual manifestation of the proton, as well as the muon and pion with no clear separation. The electron can be seen at very low energies with a approximately constant energy loss. There is a deviation between expected (Bethe-Bloch) and results, that can be associated to state of the reconstruction capabilities, where systematic uncertainties could impact. Another possibility is the “contamination" by particles do not considered.
Source: author.

- If a parameter, $\sigma$ for example, is in the “region" of the pion, the pion score is 1, if it is in the proton “region", the proton score is 1 and so on, until the score complete 2 for one of the particles.

Table 4 joins the fit parameters and established ranges for pion and proton. The criteria for the ranges was the average between pion and proton parameters. In order to test the efficiency of the tool, it is going to be used around 10,000 CC events, present in SBND sample, those match with the already discussed assumptions and the truth information about the particle of the track will be used to compare with the obtained results.

The final results are in Table 5. The muon and proton were in an acceptable efficiency of identification, given the simple as criteria used, being both over 84%. In the

Figure 30 – $dE/dx$ distribution for the topologies and particles

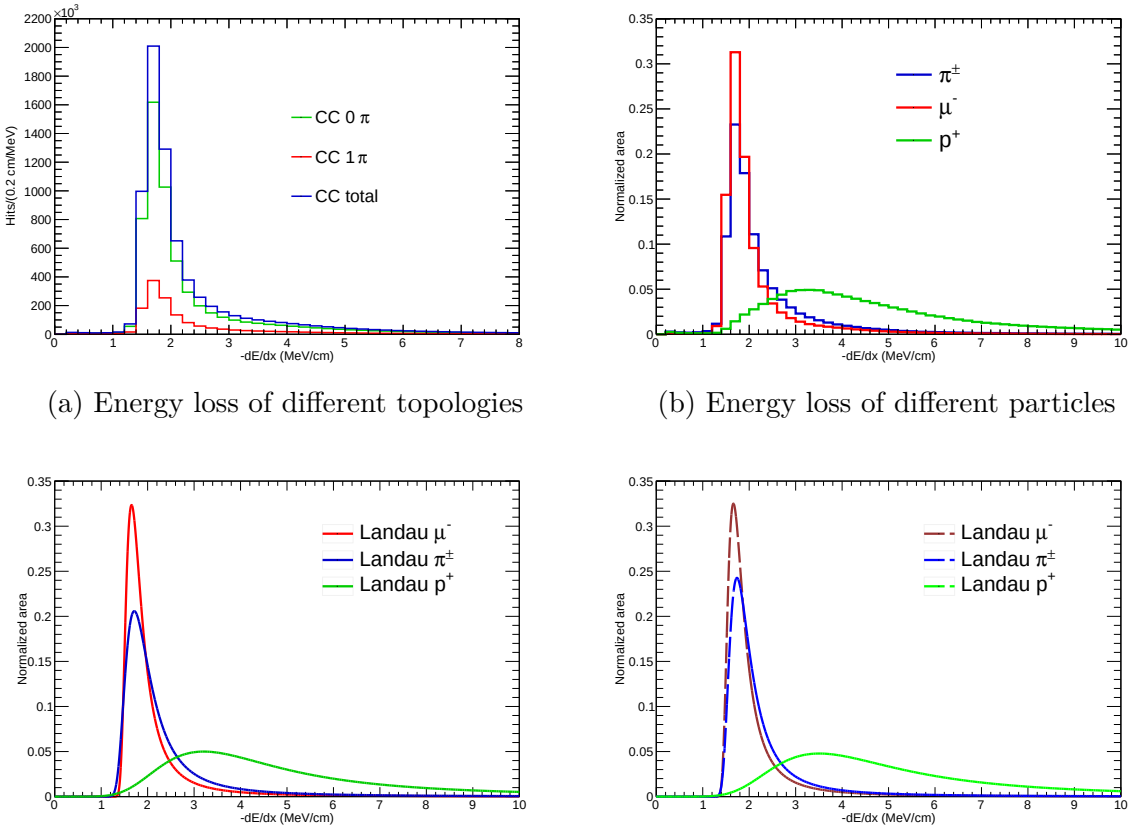


(a) Energy loss of different topologies

(b) Energy loss of different particles

(c) Landau distribution of energy loss of different particles

(d) Landau distribution of energy loss of different particles for events with $< 3$ tracks

This result remarks the high calorimetric similarity between pion and muon, which was already seen in Figures 28 and 29, as well as the large range of proton loss energy. In (c) the the Landau distribution was fitted to the three particles to understand different parameters such as $\sigma$ and height ($\chi^2_\mu = 0.02$, $\chi^2_\pi = 0.02$, $\chi^2_p = 0.01$).
Source: author.

case of the pion, was obtained a very poor capacity of identification. One hypothesis is the presence of other particles in the detector imitating the pion behavior. In general, such low efficiency indicates a needed more complete and refined choice of assumptions and a better evaluation of the tool as a whole.

Another point is the geometrical aspects of each event, that could be more explored, once the difference of angle distribution between pion and proton wasn't.

The total reconstructed energy of protons seem to have a clear cut at $\approx 0.9$ GeV in Figure 22, what indicates again a difference among pion and muon tracks with less than 2 cm.

An important point is that the normalization process makes the histogram area information get lost, which is proportional to the number of track hits. As the number of hits of any track can have a relation to a determined particle, a tunning in the selection

Figure 31 – $dE/dx$ of one CC1$\pi$ event

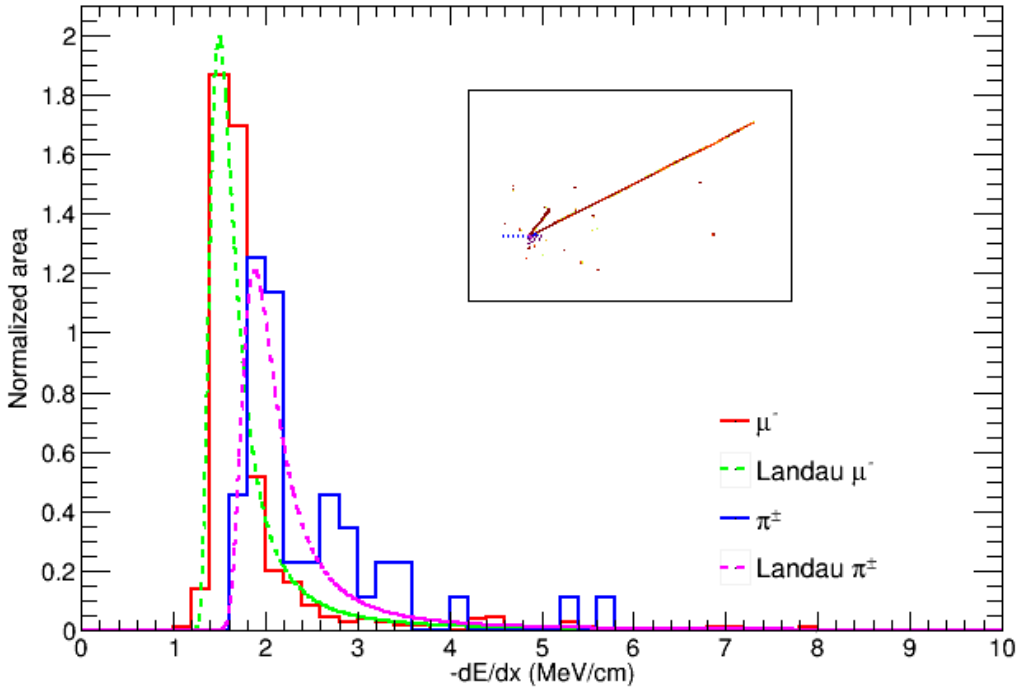


The box inside the graph contain the raw data (wires × time) of the event, with long and short tracks being muon and pion respectively. The landau distribution was fitted in both histograms with area normalized. Fitted parameters: $MPV_\mu = (1.51 \pm 0.10)$, $\sigma_\mu = (8.81 \pm 3.81) \times 10^{-2}$, $\chi^2_\mu = 0.37$, $MPV_\pi = (1.91 \pm 0.15)$, $\sigma_\pi = (0.12 \pm 0.12)$, $\chi^2_\pi = 1.20$. Source: author.

Table 4 – Parameters average for pion-proton identification distribution of 5000 CC events

| Particle | MPV | $\sigma$ | height |
|---|---|---|---|
| $\mu^-$ | $1.69 \pm 0.23$ | $0.11 \pm 0.16$ | $1.80 \pm 3.23$ |
| $\pi^\pm$ | $1.77 \pm 0.32$ | $0.15 \pm 0.19$ | $1.34 \pm 2.21$ |
| $p$ | $3.71 \pm 1.94$ | $0.90 \pm 1.11$ | $0.26 \pm 0.37$ |
| $\pi^\pm$ | $\leq 2.74$ | $\leq 0.53$ | $> 0.80$ |
| $p$ | $> 2.74$ | $> 0.53$ | $\leq 0.80$ |

The plot that represents this fit is in Figure 30d.
Source: author.

algorithm could consider the total energy loss.

Table 5 – Results of particle identification proposed

| Particle | Tries | Hits[a] | Efficiency |
|---|---|---|---|
| $\mu^-$ | 7505 | 6340 | 84.5% |
| $\pi^\pm$ | 1849 | 42 | 2.3% |
| $p$ | 1387 | 1193 | 86.0% |
| Total | 10741 | 7575 | 70.5% |

[a] The word hits here means the number of right comparisons between identification algorithm and truth information. Do not confuse to number of amount of charge detected, as discussed before.

Source: author.

A complete treatment in terms of uncertainties involved is also needed for future analysis, but the results of Table 4 indicate strong impacts, mainly in $\sigma$ and height, what can be seen as a limitation of the proposed method.

# 6 CONCLUSIONS

Neutrino interactions demonstrated to be a big source of learning particle physics and it is possible to conclude the role that neutrino-electron scattering played was a good way to understand interactions, given the shorter path in comparison to neutrino-nucleus studies. It is important to mention that BNB does not have the energy to make CC $\nu_\mu - e^-$ scatterings in SBND, given the energy threshold $\approx 11$ GeV, but the NC process is allowed even in the very low rate generated by the low magnitude of the cross section, in the order of $\approx 10^{-41}\text{cm}^2$ in comparison to neutrino-nucleus interactions, with order of $\approx 10^{-38} cm^2$ in the range of BNB. In general, these numbers mainly demonstrate that neutrinos interact very poorly, statistically speaking, no matter the medium in their way.

A better understanding of LArSoft simulation was achieved and applied in the sense of the reading tool developed in C++ and ROOT, concluding that the Monte Carlo production has been extensively tested. This represents a success for the experiment preparations as well as the goals of this study.

Even the truth information showed itself to be a powerful prediction tool, given the physics involved and can be used in cuts for separation of particles and the detector simulation with LArSoft can give unbelievable information about aspects where only in an experiment already running could achieve, testing the detection capability in many ways.

An important remark needs to be made regarding the calorimetric observables, such as $-dE/dx$, associated with secondary (or detected) particles, being a very sensitive way to identify and select secondary particles. Using it and other simple features, it was possible to select events with $\approx 70\%$ of efficiency in general, $> 80\%$ in the case of muon and proton, but it still performed poorly for the pions, given a needed set of more detailed assumptions are needed to make an acceptable particle selection tool, but the technique applied here can be useful, but yet requires a more extensive study for different particles and topologies.

The main goal of this thesis was to comprehend neutrino interactions in its fundamentals and connect this phenomena to detector physics using SBND MC simulation. The results indicated that this goal was achieved, but a very clear fact was demonstrated too: the neutrino interaction phenomena are still and open sector in physics, mainly due to its dependence on young and yet-to-be explored nuclear models. This requires a more profound study by the author. The same in the case of detection techniques, those are in fast gear in terms of particle identification and reconstruction methods, so a significant contribution would need a much more sophisticated approach. All these identifiable limitations light a clear path to be followed in my future PhD.

# REFERENCES


ABRATENKO, P. et al. Determination of muon momentum in the microboone lartpc using an improved model of multiple coulomb scattering. **Journal of Instrumentation**, v. 12, n. 10, p. 20–45, 2017. Cited on page 25.

ACCIARRI, R. et al. First observation of low energy electron neutrinos in a liquid argon time projection chamber. **Physical Review D**, v. 95, n. 7, p. 72–85, 2017. Cited on page 14.

ADAMS, C. et al. **Comparison of $\nu_\mu$-Ar multiplicity distributions observed by MicroBooNE to GENIE model predictions**. 2018. Disponível em: <https://arxiv.org/pdf/1703.06187.pdf>. Acesso em: 22 Sept. 2018. Cited on page 44.

AGUILAR, A. et al. Unexplained excess of electronlike events from a 1-gev neutrino beam. **Physical Review Letters**, v. 102, n. 10, p. 31–62, 2009. Cited on page 21.

AGUILAR, A. et al. Evidence for neutrino oscillations from the observation of $\nu$ e appearance in a $\nu$ $\mu$ beam. **Physical Review D**, v. 64, n. 11, p. 112–184, 2001. Cited on page 21.

AGUILAR, A. et al. **Observation of a Significant Excess of Electron-Like Events in the MiniBooNE Short-Baseline Neutrino Experiment**. 2018. Disponível em: <https://arxiv.org/pdf/1805.12028.pdf>. Acesso em: 10 Sept. 2018. Cited on pages 22 and 23.

AHRENS, L. et al. Measurement of neutrino-proton and antineutrino-proton elastic scattering. **Physical Review D**, v. 35, n. 3, p. 704–785, 1987. Cited on page 45.

AITCHISON, I.; HEY, A. **Gauge theories in particle physics**. Boca Raton: CRC Press, 2004. Cited on pages 26, 28, and 29.

ALKIN, A. Phenomenology of charged-particle multiplicity distributions. 2017. Disponível em: <https://arxiv.org/pdf/1710.01979.pdf>. Acesso em: 03 Jun. 2018. Cited on page 44.

ANDREOPOULOS, C. et al. **The GENIE Neutrino Monte Carlo Generator**: Physics and user manual. 2015. Disponível em: <https://arxiv.org/pdf/1510.05494.pdf>. Acesso em: 03 Jan. 2018. Cited on pages 44, 45, and 47.

ANTONELLO, M. et al. Precision measurement of the neutrino velocity with the icarus detector in the cngs beam. **Journal of High Energy Physics**, v. 2012, n. 11, p. 49–101, 2012. Cited on page 28.

ANTONELLO, M. et al. **A proposal for a three detector short-baseline neutrino oscillation program in the fermilab booster neutrino beam**. Batavia, 2015. Disponível em: <https://arxiv.org/pdf/1503.01520.pdf>. Acesso em: 12 Feb. 2018. Cited on pages 13, 14, 22, 23, 24, 43, and 47.

BILENKY, S. Neutrino in standard model and beyond. **Physics of Particles and Nuclei**, v. 46, n. 4, p. 475–496, 2015. Cited on page 13.

BODEK, A.; YANG, U. Higher twist, ξw scaling, and effective lo pdfs for lepton scattering in the few gev region. **Journal of Physics G: Nuclear and Particle Physics**, v. 29, n. 8, p. 1861–1899, 2003. Cited on page 45.

CARENA, M. et al. Invisible z-boson decays at e+ e- colliders. **Physical Review D**, v. 68, n. 11, p. 113–156, 2003. Cited on page 13.

CHURCH, E. D. **Larsoft: A software package for liquid argon time projection drift chambers**. 2013. Disponível em: <https://arxiv.org/pdf/1311.6774.pdf>. Acesso em: 5 May 2018. Cited on page 47.

COLLIN, G. et al. First constraints on the complete neutrino mixing matrix with a sterile neutrino. **Physical review letters**, v. 117, n. 22, p. 22–38, 2016. Cited on page 21.

CONRAD, J.; SHAEVITZ, M. **Sterile Neutrinos: An Introduction to Experiments**. 2016. Disponível em: <https://arxiv.org/pdf/1609.07803.pdf>. Acesso em: 12 Dec. 2017. Cited on page 21.

DECAMP, D. et al. Determination of the number of light neutrino species. **Physics Letters B**, v. 231, n. 4, p. 519–529, 1989. Cited on page 13.

FOGLI, G. et al. Solar neutrinos (with a tribute to john. n. bahcall). 2006. Disponível em: <https://arxiv.org/pdf/hep-ph/0605186.pdf>. Acesso em: 2 Aug. 2018. Cited on page 16.

FORMAGGIO, J. A.; ZELLER, G. From ev to eev: neutrino cross sections across energy scales. **Reviews of Modern Physics**, v. 84, n. 3, p. 1307–1337, 2012. Cited on pages 43, 44, and 45.

FROGGATT, C. D.; MUHEIM, F.; SMITH, P. F. **Neutrinos in particle physics, astrophysics and cosmology**. Boca Raton: CRC Press, 2008. Cited on page 13.

GANDHI, R. et al. Neutrino interactions at ultrahigh energies. **Phys. Rev. D**, v. 58, p. 93–108, 1998. Disponível em: <https://link.aps.org/doi/10.1103/PhysRevD.58.093009>. Cited on page 13.

GEANT, C. et al. **Geant4 user's guide for application developers**. 2012. Disponível em: <http://216.165.129.135/distfiles/BookForAppliDev-4.10.03.pdf>. Acesso em: 15 May 2018. Cited on page 47.

GOLLAPINNI, S. **Neutrino Cross section Future**. 2016. Disponível em: <https://arxiv.org/pdf/1602.05299.pdf>. Acesso em: 22 Mar. 2018. Cited on page 25.

GREEN, C. et al. The art framework. **Journal of Physics: Conference Series**, v. 396, n. 2, p. 10–22, 2012. Cited on page 47.

GREINER, W. **Relativistic Quantum Mechanics**: Wave equations. Berlin: Springer Science & Business Media, 2013. Cited on page 29.

GRIFFITHS, D. **Introduction to Particle Physics**. 2. ed. New Jersey: J. Wiley & Sons, Inc, 2008. Cited on pages 15, 26, 28, 30, 31, 34, 35, 39, and 41.

HANNEKE, D.; FOGWELL, S.; GABRIELSE, G. New measurement of the electron magnetic moment and the fine structure constant. **Physical Review Letters**, v. 100, n. 12, p. 120–141, 2008. Cited on page 29.

LANCASTER, T.; BLUNDELL, S. J. **Quantum field theory for the gifted amateur**. Oxford: OUP Oxford, 2014. Cited on page 35.

LANDAU, L.; LIFSHITZ, E. **Quantum mechanics**. 3. ed. Oxford: Pergamon Press, 1977. Cited on page 27.

LEO, W. R. **Techniques for nuclear and particle physics experiments**: a how-to approach. Berlin: Springer Science & Business Media, 2012. Cited on pages 32 and 53.

LUZIO, V. P. **Uso de detectores de radiação de fluorescência atmosférica no estudo de raios cósmicos de ultra-alta energia**. 2016. 166 f. Dissertação (Masters in Physics) — UFABC, São Paulo, 2016. Cited on page 53.

MINIBOONE, C. et al. **The Neutrino Flux prediction at MiniBooNE**. 2008. Disponível em: <https://arxiv.org/pdf/0806.1449.pdf>. Acesso em: 12 Apr. 2017. Cited on pages 21 and 22.

NAGASHIMA, Y. **Elementary particle physics**. [s.n.], 2010. Disponível em: <https://inis.iaea.org/search/search.aspx?orig_q=RN:41105891>. Acesso em: 30 Jun. 2018. Cited on pages 27 and 28.

NEWTON, I. Letter to robert hooke. **February**, v. 5, p. 1675–1681, 1675. Cited on page 9.

PALAMARA, O. Neutrino detection in the argoneut lar tpc. **Journal of Physics: Conference Series**, v. 408, n. 1, p. 120–127, 2013. Cited on page 44.

PARTYKA, K. A. **Exclusive Muon-Neutrino Charged Current Muon Plus Any Number of Protons Topologies In ArgoNeuT**. 2013. 186 f. Tese (Doutorado), 2013. Disponível em: <http://inspirehep.net/record/1373857/files/fermilab-thesis-2013-40.pdf>. Acesso em: 13 Apr. 2018. Cited on pages 25, 44, and 47.

PATRIGNANI, C.; GROUP, P. D. et al. Review of particle physics. **Chinese physics C**, v. 40, n. 10, p. 1–211, 2016. Cited on pages 18, 21, and 23.

REIN, D.; SEHGAL, L. M. Neutrino-excitation of baryon resonances and single pion production. **Annals of Physics**, v. 133, n. 1, p. 79–153, 1981. Cited on page 45.

REIN, D.; SEHGAL, L. M. Coherent $\pi^0$ production in neutrino reactions. **Nuclear Physics B**, v. 223, n. 1, p. 29–44, 1983. Cited on page 45.

SMITH, C. L. Neutrino reactions at accelerator energies. **Phys. Rept.**, v. 3, n. 0958, p. 261–379, 1971. Cited on page 44.

SNO, C. et al. **Electron Energy Spectra, Fluxes, and Day-Night Asymmetries of B Solar Neutrinos from the 391-Day Salt Phase SNO Data Set**. 2005. Disponível em: <https://arxiv.org/pdf/nucl-ex/0502021.pdf>. Acesso em: 1 Jul. 2018. Cited on pages 15 and 16.

SONG, X.-K. et al. **Quantifying Quantum Coherence in Experimentally-Observed Neutrino Oscillations**. 2018. Disponível em: <https://arxiv.org/pdf/1806.00715.pdf>. Acesso em: 08 Sept. 2018. Cited on page 19.

STEANE, A. M. **An introduction to spinors**. 2013. Disponível em: <https://arxiv.org/pdf/1312.3824.pdf>. Acesso em: 2 May 2018. Cited on pages 29 and 33.

VALDIVIESSO, G. A. **Novos limites para violação do princípio da equivalência em neutrinos solares**. 2008. 138 f. Tese (PhD in Physics) — Unicamp, Campinas, 2008. Cited on pages 15 and 18.

VALDIVIESSO, G. d. A. **Introdução à fenomenologia da oscilação de neutrinos, no vácuo e na matéria**. 2004. 114 f. Dissertação (Masters in Physics) — Unicamp, Campinas, 2004. Cited on pages 13 and 15.

WANG, T. C. **New Physics at the neutrino oscillation frontier**. 2018. 120 f. Tese (PhD in Philosophy) — Durham University, Durhan, 2018. Cited on page 13.

WENTZ, J. et al. Simulation of atmospheric muon and neutrino fluxes with corsika. **Physical Review D**, v. 67, n. 7, p. 73–89, 2003. Cited on page 46.

# APPENDIX A - Structure of C++ file able to read the ROOT file and selection algorithm used

The general structure of the C++ file (“macro.cpp") able to read and analyzes the ROOT file where the simulation sample was in. This is a summary of the original file.

```
#include <iostream.h>
#include <iostream>
#include <string>
#include <typeinfo>
#include <algorithm>
#include "TTree.h"
#include "TChain.h"
#include "TNtuple.h"
#include "TFile.h"
#include "TBranch.h"
#include "TH1D.h"

using namespace std;

void macro(){

//opening ROOT file
TFile *my_file = new TFile("anatree50000.root","READ");
//opening the tree in the file (TTree)
TTree *myReader = (TTree*) my_file->Get("analysistree/anatree");

//declaring the variables
Int_t variable1;//...
Float_t variable2;//...
Double_t variable3;//...
Short_t variable4;//...

//declaring histograms
TH1D *histogram = new TH1D("histogram","",50,0,10);
```

```
30 //                    .
31 //                    .
32 //                    .
33
34 Long64_t nentries = myReader->GetEntriesFast();
35
36 //collecting branches from tree file (ROOT file)
37 myReader->SetBranchAddress("run",&run);
38 myReader->SetBranchAddress("genie_primaries_pdg",&genie_primaries_pdg);
39 myReader->SetBranchAddress("geant_list_size",&geant_list_size);
40 myReader->SetBranchAddress("trkpidpdg_pmalgtrackmaker",&
       trkpidpdg_pmalgtrackmaker);
41 //                    .
42 //                    .
43 //                    .
44 //getting the first event
45 myReader->GetEntry(0);
46 //loop over all 50000 events from ROOT file
47 for(int j=0; j<nentries; j++){ //Read each event
48   myReader->GetEntry(j); //Read branches from the event
49
50   nmuons = 0;
51   npions = 0;
52   nprotons = 0;
53
54   nmuons_g4 = 0;
55   npions_g4 = 0;
56   nprotons_g4 = 0;
57
58   //Counting GENIE particles with TRUTH information: loop over genie
       primaries
59   for(int genie=0;genie<genie_no_primaries;genie++){
60     if(genie_status_code[genie] == 1 && genie_primaries_pdg[genie] == 13)
      nmuons++;
```

```
61    if(genie_status_code[genie] == 1 && abs(genie_primaries_pdg[genie] ==
      211)) npions++;
62    if(genie_status_code[genie] == 1 && genie_primaries_pdg[genie] == 2212)
      nprotons++;
63  }
64
65  //Counting GEANT4 particles with TRUTH information: loop over geant
      primaries
66  for(int geant=0;geant<geant_list_size_in_tpcAV;geant++){
67    if(process_primary[geant] == 1 && pdg[geant] == 13) nmuons_g4++;
68    if(process_primary[geant] == 1 && abs(pdg[geant]) == 211) npions_g4++;
69    if(process_primary[geant] == 1 && pdg[geant] == 2212) nprotons_g4++;
70  }
71
72  //==================SELECTION ALGORITHM=====================================
73  //if genie and geant nparticles are equal
74  if(nmuons==nmuons_g4 && npions==npions_g4 && nprotons==nprotons_g4){
75    //if the event is CC and the number of pion is < 2
76    if(nmuons == 1 && npions < 2){
77      //if the number of tracks is 0 or > 2, skip this loop
78      if(ntracks_pmalgtrackmaker == 0 || ntracks_pmalgtrackmaker > 2)
      continue;
79
80    // Loop over tracks of the event
81    for(int track=0;track<ntracks_pmalgtrackmaker;track++){
82      //if the track has less than 2 cm or more than 15 m, skip this loop
83      if(trkrange_pmalgtrackmaker[track][2] < 2 || trkrange_pmalgtrackmaker
      [track][2] > 1500) continue;
84      //loop over track hit
85      for(int trkhit=1;trkhit<ntrkhits_pmalgtrackmaker[track][2];trkhit++){
86        // Loop over hits of the track
87        //filling a temporary histogram
88        dEdx_track->Fill(trkdedx_pmalgtrackmaker[track][2][trkhit]);
89      }//end loop over track hits
90      //if the event has only one track this is a muon
```

```
91      if(ntracks_pmalgtrackmaker == 1){
92        //comparing to TRUTH information
93        if(trkpdgtruth_pmalgtrackmaker[track][2] == 13){
94        nAcer++;//hit total
95        nmuAcer++;//hit muon
96        }
97        nTent++;
98        nmuTent++;
99      }
100     //if the event has 2 tracks
101     else if(ntracks_pmalgtrackmaker == 2){
102       //normalizing histogram
103       dEdx_track->Scale(norm/dEdx_track->Integral(), "height");
104       //first guess
105       landau_mu->SetParameters(1,2,0.1);
106       //Fitting
107       dEdx_track->Fit(landau_mu,"0 Q MW");
108       //collecting Landau parameters
109       height2[track] = landau_mu->GetParameter("height");
110       peak2[track] = landau_mu->GetParameter("peak");
111       width2[track] = landau_mu->GetParameter("width");
112       //if already passed for all tracks
113       if(track == 1){
114         //is the muon is in the position 0
115         if(trklen_pmalgtrackmaker[0] > trklen_pmalgtrackmaker[1]){
116           //comparing to TRUTH information
117           if(trkpdgtruth_pmalgtrackmaker[0][2] == 13){
118             nAcer++;
119             nmuAcer++;
120             nmuTent++;
121           }
122           else{
123             nmuTent++;
124           }
125           //height
```

```
126             if(height2[1] > 0.8) score_pi++;
127             if(height2[1] <= 0.8) score_pro++;
128             //width
129             if(width2[1] <= 0.53) score_pi++;
130             if(width2[1] > 0.53) score_pro++;
131             //peak
132             if(peak2[1] <= 2.74) score_pi++;
133             if(peak2[1] > 2.74) score_pro++;
134             //if the pion score > than proton score it is a pion
135             if(score_pi > score_pro){
136               //comparing to TRUTH information
137               if(abs(trkpdgtruth_pmalgtrackmaker[1][2]) == 211){
138                 nAcer++;
139                 npiAcer++;
140                 npiTent++;
141               }
142               else{
143                 npiTent++;
144               }
145             }
146             else{
147               //it is a proton
148               //comparing to TRUTH information
149               if(abs(trkpdgtruth_pmalgtrackmaker[1][2]) == 2212){
150                 nAcer++;
151                 nproAcer++;
152                 nproTent++;
153               }
154               else{
155                 nproTent++;
156               }
157             }
158
159           }
160           else{
```

```
161             //comparing to TRUTH information
162             if(trkpdgtruth_pmalgtrackmaker[1][2] == 13){
163               nAcer++;
164               nmuAcer++;
165               nmuTent++;
166             }
167             else{
168               nmuTent++;
169             }
170             //altura
171             if(height2[0] > 0.8) score_pi++;
172             if(height2[0] <= 0.8) score_pro++;
173             //largura
174             if(width2[0] <= 0.53) score_pi++;
175             if(width2[0] > 0.53) score_pro++;
176             //pico
177             if(peak2[0] <= 2.74) score_pi++;
178             if(peak2[0] > 2.74) score_pro++;
179
180             //if pion score > proton score
181             if(score_pi > score_pro){
182               //comparing to TRUTH information
183               if(abs(trkpdgtruth_pmalgtrackmaker[0][2]) == 211){
184                 nAcer++;
185                 npiAcer++;
186                 npiTent++;
187               }
188               else{
189                 npiTent++;
190               }
191             }
192             //if the pion score < than proton score it is a proton
193             else{
194               //comparing to TRUTH information
195               if(abs(trkpdgtruth_pmalgtrackmaker[0][2]) == 2212){
```

```
196                 nAcer++;
197                 nproAcer++;
198                 nproTent++;
199               }
200               else{
201                 nproTent++;
202               }
203             }
204           }
205           //tries
206           nTent++;
207           nTent++;
208         }//end counting track == 1
209       }//end number of tracks = 2
210       //returning scores to 0
211       score_pi = 0;
212       score_pro = 0;
213       //reseting histogram
214       dEdx_track->Reset("ICESM");
215     }//end loop over tracks
216    }//end CC
217  }//end geant == genie
218 }//end ntuples
219
220 //display the results
221 cout <<"Total tries:" << nTent << "\t" << "Total hits:" << nAcer << endl;
222 cout <<"Tries muon:" << nmuTent << "\t" << "Hits muon:" << nmuAcer << endl;
223 cout <<"Tries pion:" << npiTent << "\t" << "Hits pion:" << npiAcer << endl;
224 cout <<"Tries proton:" << nproTent << "\t" << "Hits proton:" << nproAcer <<
      endl;
225
226 //creating a window
227 TCanvas *c1 = new TCanvas("c1","c1");
228 //histogram configurations...
229 histogram->Draw();
```

```
230
231 TLegend* legend;
232 //legend configurations...
233 legend->Draw();
234
235 //saving histograms
236 c1->SaveAs("C:/path/of/the/file.pdf");
237
238 }//end
```